MASTERARBEIT | MASTER'S THESIS

Titel | Title

Molecular Dynamics Simulations of the GNB1 Encephalopathy-Associated A92T Mutation in the Gβ1γ2 Dimer in Complex with Gαi and GRK2

verfasst von | submitted by

Sabine Bürger BSc

angestrebter akademischer Grad | in partial fulfilment of the requirements for the degree of

Magistra pharmaciae (Mag. pharm.)

Wien | Vienna, 2025

Studienkennzahl lt. Studienblatt | Degree programme code as it appears on the student record sheet:	UA 066 605
Studienrichtung lt. Studienblatt | Degree programme as it appears on the student record sheet:	Masterstudium Pharmazie
Betreut von | Supervisor:	Assoz. Prof. Mag. Dr. Anna Weinzinger Privatdoz.

Acknowledgements

First of all, I would like to express my deepest gratitude to Assoc.-Prof. Mag. Dr. Anna Weinzinger, Privatdoz., for welcoming me into her research group and supervising this master's thesis. I am glad to have had the opportunity to be part of such a wonderful and supportive team. Additionally, I want to thank Ilia Steshin for his guidance throughout this process. I truly appreciate everything you have done to support me as well as all the other master students whenever we needed help.

Words cannot express how grateful I am for my family and friends. None of this would have been possible without your continuous support and encouragement. Thank you to my fellow students for all the precious moments we got to share throughout this journey – with you, everything was much easier to endure.

I am forever thankful to have such an amazing support system. Thank you!

Abstract

GNB1 encephalopathy is a rare genetic disorder caused by pathogenic mutations in the *GNB1* gene. *GNB1* encodes for the $G\beta_1$ subunit of heterotrimeric G proteins, which play a crucial role in intracellular signal transduction. Disruption of these signalling pathways leads to various neurodevelopmental symptoms, though the presented phenotype often varies. In this thesis, the disease-causing variant A92T is examined in greater detail. One literature reported patient presents with global developmental delay, intellectual disability, muscular hypotonia, seizures, cerebellar hypoplasia, and ataxia. In previous studies, this variant has been found to display abnormal signal transmission behaviour. In the course of this thesis, several molecular dynamic simulations have been conducted in order to investigate the structural and functional consequences the A92T mutation has on heterotrimer formation between $G\beta_1\gamma_2$ with $G\alpha_i$ as well as the interaction of the dimer with GRK2, which plays an important role in signal termination. Free energy calculations, root mean square deviation (RMSD), root mean square fluctuation (RMSF), and residue energy analysis have been performed for this purpose. The results suggest moderate complex destabilisation for the examined $G\alpha_iG\beta_1\gamma_2$ trimer, and no changes in stability for the $G\beta_1\gamma_2$GRK2 complex. These findings align with previous functional assays as well as provide additional details from an atomistic perpective. However, further investigation in regard to the several other downstream signalling pathways needs to be done in order to fully understand the underlying pathology – and find potential druggable targets.

Zusammenfassung

GNB1-Enzephalopathie ist eine seltene genetische Erkrankung, die durch pathogene Mutationen im *GNB1*-Gen verursacht wird. *GNB1* kodiert für die $G\beta_1$-Untereinheit heterotrimerer G-Proteine, die eine entscheidende Rolle bei der intrazellulären Signalübertragung spielen. Eine Störung dieser Signalwege führt zu verschiedenen neurologischen Entwicklungsstörungen, wobei der auftretende Phänotyp jedoch häufig variiert. In dieser Arbeit wird die krankheitsverursachende Variante A92T genauer untersucht. Eine in der Literatur beschriebene Patientin leidet unter einer allgemeinen Entwicklungsverzögerung, intellektueller Beeinträchtigung, Muskelhypotonien, Krampfanfälle, Kleinhirnhypoplasie und Ataxie. In früheren Studien wurde festgestellt, dass diese Variante ein abnormales Signalübertragungsverhalten aufweist. Im Rahmen der vorliegenden Arbeit wurden mehrere molekulardynamische Simulationen durchgeführt, um die strukturellen und funktionellen Auswirkungen der A92T-Mutation auf die Heterotrimerbildung zwischen $G\beta_1\gamma_2$ und $G\alpha_i$ sowie die Interaktion des Dimers mit GRK2, welches eine wichtige Rolle bei der Signalbeendigung spielt, zu untersuchen. Zu diesem Zweck wurden Berechnungen der freien Energie, der quadratischen Mittelwertabweichung (RMSD), der quadratischen Mittelwertfluktuation (RMSF) und eine Analyse der Energien einzelner Aminosäuren durchgeführt. Die Ergebnisse deuten auf eine mögliche Komplexdestabilisierung für das untersuchte $G\alpha_iG\beta_1\gamma_2$-Trimer hin, während keine Veränderungen in der Stabilität des $G\beta_1\gamma_2$GRK2-Komplexes festgestellt wurden. Diese Ergebnisse stimmen mit früheren Funktionsassays überein und liefern zusätzliche Details aus atomistischer Perspektive. Es sind jedoch weitere Untersuchungen hinsichtlich der verschiedenen anderen nachgeschalteten Signalwege erforderlich, um die zugrunde liegende Pathologie vollständig zu verstehen – und potentielle Wirkstoffziele zu finden.

Table of Contents

List of Figures

List of Tables

1. Introduction

As knowledge on neurodevelopmental diseases is growing, *de novo* mutations in neuronally expressed genes have been found to frequently cause conditions like global developmental delay (GDD). These often coincide with intellectual disability (ID), seizures, and other features, making it not only genetically highly heterogeneous but clinically as well [1]. Mutations in genes encoding for guanine nucleotide-binding proteins (G proteins) such as the *GNB1* gene have, for example, been described to result in GDD and ID. G proteins are ubiquitously expressed, therefore such diseases affect not only brain function, but cause a variety of different symptoms [2].

1.1. G Protein-Coupled Receptors

1.1.1. Signalling Pathway

In order to understand how mutations in the *GNB1* gene influence G protein function, it is necessary to first consider how this signalling pathway works.

The family of G protein-coupled receptors (GPCRs) is the largest within seven transmembrane domain receptors and conduct important cellular functions like neuronal signalling as well as cell proliferation, development, and survival [3]. They activate biochemical reaction cascades that subsequently modify the function of various target proteins [4].

Heterotrimeric G proteins are made up of three subunits, namely Gα, β, and γ with all of them having different isoforms as well. In humans, there are 16 distinct genes encoding for Gα subunits, 5 for Gβ variants, and 12 for different Gγ subunits, allowing for a wide range of possible G protein combinations [5, 6, 7]. These proteins transmit the actions of numerous cell surface receptors after binding of an extracellular signal. Following G

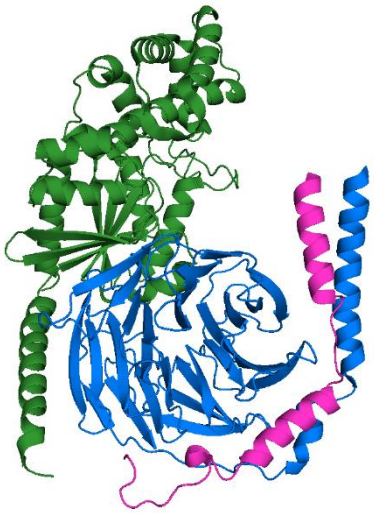

Figure 1: $G\alpha_i G\beta_1\gamma_2$ complex (PDB ID 1GP2) shown in PyMOL. Green: $G\alpha_i$; blue: $G\beta_1$; pink: $G\gamma_2$.

protein activation, Gα acts as a monomer while Gβγ stays obligatorily coupled in a dimeric form. When in the resting state, GDP is bound to Gα, allowing the trimer Gαβγ ($G\alpha_i G\beta_1\gamma_2$ illustrated in Figure 1) to bind to its receptor. Upon receptor activation, GDP gets replaced with GTP, causing conformational changes in the α subunit. This leads to dissociation from the βγ complex and exposure of possible interaction surfaces on Gβγ. Both Gα and Gβγ can then interact with downstream effector molecules like phospholipases and ion channels. This enables them, among other things, to influence the membrane potential of the cell [4, 5]. In addition, Gβγ dimers are not strictly membrane-bound, as the type of Gγ prenylation influences their translocation dynamics. They are able to relocate to intracellular compartments such as the Golgi apparatus, providing opportunities for interactions with cytosolic effector proteins [8].

G proteins are activated not only by GPCR stimulation but also by proteins called nonreceptor activators of G protein signalling (AGS). They act through different mechanisms, with some influencing GDP/GTP exchange on Gα subunits, and others modulating signalling via interactions with Gβγ [8].

Signal termination works reversely by exchanging Gα-bound GTP for GDP, again allowing the formation of the inactive trimer Gαβγ. The α subunit has an intrinsic capability to hydrolyse GTP which can also be modulated by regulators of G protein signalling (RGS proteins) by binding to Gα and increasing the rate of GTP hydrolysis [5]. However, this mechanism alone is not sufficient to completely erase a received signal, because the active receptor is still able to reactivate the G protein. In order to avoid this, the βγ dimer interacts with G protein-coupled receptor kinases (GRKs), e.g. GRK2, which in turn phosphorylate intracellular receptor domains of GPCRs. Another regulator of cellular signal transduction, arrestin, can then bind to these phosphorylated segments and block the receptor for G protein interactions. This process is called homologous desensitisation and protects the cell from overstimulation. Marking of receptors with arrestin also targets the receptor for clathrin-mediated endocytosis, thus leading to downregulation of these signalling pathways. Coupling of Gβγ and GRKs also hinders GPCR signal transmission by simply blocking interactions with effector targets [9, 10]. In this context, the affinity between GRKs and Gβγ dimers plays an important role in efficient membrane recruitment of GRK and subsequent signal termination [11].

1.1.2. $G\beta_1$ Structure

The $G\beta_1$ subunit assumes a propeller-like structure composed of seven blades, each consisting of four antiparallel β-strands that are highly conserved (illustrated in Figure 2). At its N-terminus, the protein features a 25-residue α-helical domain followed by a connecting loop that links the helix to the propeller framework [8]. This α-helix forms a tight interaction with the γ subunit of the dimer. Interaction with the α subunit of the G protein is mediated by two distinct regions. The N-terminal α-helix of Gα associates with blade 1 at

the side of the β-propeller, while the switch II region, which rearranges upon GTP binding, engages the upper surface of the β-propeller [5].

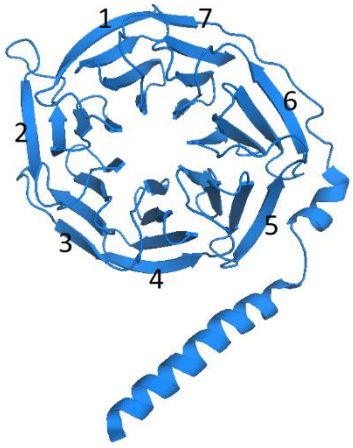

Figure 2: Gβ$_1$ subunit (extracted from PDB ID 1GP2) shown in PyMOL. Propeller blades numbered 1-7.

1.2. *GNB1* Encephalopathy

1.2.1. Pathogenesis

GNB1 encephalopathy (*GNB1*-E), also known as *GNB1*-related neurodevelopmental disorder or *GNB1* syndrome, is a rare occurring autosomal dominant genetic disease caused by missense, frameshift, or splice-site variants in the Gβ$_1$ subunit-encoding *GNB1* gene [3, 12, 13, 14]. The latest research findings from 2024 describe only about 68 confirmed cases worldwide [12] with more than 25 different mutations characterised as the cause of disease [15, 16].

Most documented cases of the condition have been linked to pathogenic *de novo* missense mutations in the *GNB1* gene [3, 17]. They are predominantly located in exons 5-7, suggesting the existence of a mutational hotspot. A case report, published in 2021 by Da Silva and colleagues, states that 88% of all identified missense mutations are located in exons 6 and 7. Furthermore, 25% of the cases described at the time were found to carry one specific variant (I80T), which provides additional support for this hypothesis. The region of exons 5-7 plays a key role in mediating interactions between Gβ$_1$γ and Gα [2, 17], as well as other binding partners. Disruption of these interactions is thought to disturb the regulation of signalling cascades, which in turn can manifest as gain-of-function, dominant negative, or loss-of-function outcomes, depending on the specific molecular alteration [18].

The amino acid sequence of *GNB1* is identical across humans and other mammals (e.g., mouse, rat, bovine), even differing from zebrafish by only four amino acid residues. This substantial evolutionary conservation suggests strong selective pressure against

variation, implying that even minor sequence alterations may interfere with the protein structure, impair function [2] and result in disease [17].

1.2.2 Clinical Picture

GNB1 is ubiquitously expressed [2] and mutations therefore show a wide range of clinical manifestations. As mentioned before, GDD and ID as well as hypotonia are lead symptoms in *GNB1*-E and vary in severity [12]. All but one documented patient case reports present with moderate to severe GDD [1], and 74% are described to display ID, though it is important to mention that at the time of publication, cognitive function could not be reliably evaluated in a number of individuals due to young age [18].

Although a potential influence cannot be ruled out, no evidence has been reported on the impact of *GNB1*-E on pregnancy or childbirth. First symptoms may occur during the neonatal period, manifesting as feeding difficulties [12]. This can result in poor weight gain, yet the majority of affected individuals eventually outgrew their difficulties [18]. Over time, GDD becomes increasingly apparent as most patients are either unable to achieve independent walking skills or demonstrate delayed onset. In certain cases, patients experience severe movement impairments, such as hemiplegia, spastic diplegia, or dyskinetic quadriplegia [12].

In around 40% of *GNB1*-E cases, individuals are nonverbal [18]. Among patients who are able to speak, expressive language is more impaired than receptive abilities, with restricted vocabulary and frequent dysarthria [12]. In three cases, developmental regression of varying manifestations was reported [18].

Other possible neurological symptoms include: muscle tone or movement disorders, epilepsy, eye movement disorders, and sensory impairment. Muscle tone disorders are very common among *GNB1* patients and are often characterised by infantile hypotonia (present in approximately 70% of cases), which may progresses to spastic hypertonia with age, or hypotonia persists. The most frequently reported movement disorder is dystonia, with onset ranging from 2 to 16 years of age. Further manifestations are ataxia, tics, and chorea [12].

Epilepsy has been tested for in 51 patients, of which 27 (53%) were diagnosed with some form of seizure disorder. A spectrum of different seizure types is exhibited, comprising epileptic spasms as well as tonic, myoclonic, generalised tonic-clonic, absence, and focal seizures [18]. Important to note is that in some patients, symptoms only occur at a certain age, for some they worsen over time, for others they improve gradually, making it a very complex aspect of the disease [14, 19]. *GNB1*-E is also linked to West syndrome [18], an infantile spasms syndrome defined by hypsarrhythmia, clustered spasms, and developmental delay or regression [20].

Regarding ocular anomalies, nystagmus is the most prevalent, being present in 36-46% of individuals. Other findings include strabismus, ophthalmoplegia, gaze deviation,

upward gaze palsy, continuous reverse ocular dipping, and slow ocular pursuit response. In 11% of patients, visual impairment related to cortical visual dysfunction or optic nerve atrophy has been documented [12, 18]. Two recently confirmed cases and one suspected case of rod-cone dystrophy have been described in patients with *GNB1* variants. Since $G\beta_1$ is highly expressed in rod photoreceptor cells of the retina as a subunit of transducin, a protein crucial for the phototransduction process, this raises the possibility of a causal association [21, 22].

Another form of sensory impairment, though far less common, is sensorineural hearing loss, which can affect either one or both sides. One individual suffered not only from severe sensorineural hearing impairment, but conductive hearing loss as well. A brain MRI of another patient showed hypoplasia of the right cochlear nerve [14, 18].

In some patients, there have also been other abnormal brain MRI discoveries, such as delayed or abnormal myelination, corpus callosum anomalies, cerebral volume loss, ventriculomegaly, and bilateral polymicrogyria [18].

36 individuals have been tested for behavioural issues of which 42% show attention-deficit/hyperactivity disorder (ADHD), autism spectrum disorder (ASD), or repetitive and stereotypic habits [18]. Bouts of aggressive behaviour have also been recognised in some patients [2, 17, 19].

There are also less frequently described clinical features associated with *GNB1*-E like gastrointestinal problems, genitourinary abnormalities in males, cardiovascular deformities, craniofacial anomalies, or hypothyroidism [18]. Cutaneous mastocytosis has been diagnosed in four cases, suggesting a possible link between mast cell disease and abnormal GPCR downstream signalling caused by GNB1 variants [3, 14].

1.2.3 Malignancy

Gain-of-function variants of Gα have already been reported in numerous cancer types, but oncogenic mutations in Gβ subunits had not been investigated until Yoda et al. published a 2015 study showing that some somatic missense mutations convey cytokine-independent growth. They identified recurring mutations in patients with hematologic malignancies that affect amino acid residues K57, K78, I80, K89, and M101, which are located on the Gα subunits and downstream effector interaction site of the protein. In particular, K89E has been extensively tested and confirmed to convey cytokine- as well as interleukin 3 (IL3)-independent growth. This mutation along with the variants I80T and K57E were found to exhibit reduced binding to all Gα subunits tested *in vitro*, and caused myeloid malignancies *in vivo* in mouse bone marrow transplantation experiments. Oncogenic Gβ mutations have been identified in multiple cancers, and trigger canonical G protein signalling by interfering with Gα/Gβγ interactions [23]. In 2017, Brett et al. reported a patient with clinical features of *GNB1*-E and acute lymphoblastic leukaemia (ALL)

carrying a G77A variant [24]. These findings indicate a possible correlation between selected pathogenic *GNB1* variants and an increased chance for malignancies [18].

1.2.4 Prognosis

Life expectancy is difficult to determine, as most documented cases involve children or young adults. Nonetheless, reports of adult individuals with *GNB1*-E – though limited in number – demonstrate that reaching adulthood is possible [12]. Because advanced genetic analyses are often lacking in adults with disabilities, affected individuals are likely underestimated and underreported. However, since congenital anomalies typically linked to high morbidity and mortality are missing, the long-term outlook appears positive under adequate supportive management [18].

1.2.5 Treatment

As of now, there is no causal therapy for *GNB1*-E. Management is therefore symptomatic and relies on multidisciplinary approaches, largely guided by anecdotal evidence. Non-pharmacological treatment options include physiotherapy and occupational therapy, aiming to prevent contractures, falls, and spasticity-related complications. Depending on the individual phenotype, additional measures may involve support from sensory impairment specialists, psychotherapy, and use of walking aids [12]. In two patients with communication difficulties but no hearing deficits, progress was achieved through alternative forms of expression, such as sign language [18].

Pharmacological intervention is individualised, as drug responses vary considerably, and is primarily indicated for epilepsy, dystonia, or movement disorders. Epilepsy is treated with standard anti-seizure medication with no explicit drug preference [12]. As listed in Table 1, different drug combinations are being used, however, adequate control is not achieved in every patient [14]. Dystonia management typically involves conventional pharmacologic therapy as well, including anticholinergic drugs, dopaminergic agents (agonists, antagonists, and depleters), benzodiazepines, or baclofen. In addition, deep brain stimulation has shown benefit in one reported case, and was trialed in another [12].

Symptoms	Patient 3	Patient 5	Patient 8	Patient 11	Patient 13	Patient 18	Individual 2, Petrovski et al. (2016)
Mutation (GRCh37; GenBank: NM_002074.4)	Chr1:1735947C > T	Ch1:1737942A > G	Chr1:1737942A > G	Chr1:1737942A > G	Chr1:1737942A > G	Chr1:1737942A > G	chr1: g.1737948 T > C
	c.341G > A	c.239 T > C	c.239 T > C	c.239 T > C	c.239 T > C	c.239 T > C	c.233A > G
	p.Cys114Tyr	p.Ile80Thr	p.Ile80Thr	p.Ile80Thr	p.Ile80Thr	p.Ile80Thr	p.Lys78Arg
EEG	3 years: Right and left temporal epileptiform discharges during sleep (T7-T8) and left temporal slowing	1 years.: Normal; 6 years: Centroparietal rt + lt epileptiform activity with significant increase during sleep (ESES)	3 years: Normal; 4.5 years: Presence of Ictal activity during sleep, and wake characterized by high waves and generalized slow waves	11 years: Infrequent, brief, independent right and left frontal / fronto-central sharp wave discharges suggestive of multi-focal epilepsy	2 years: Normal	4 years and 9 years: Focal epileptiform activity with important persistence in wakefulness that is strikingly activated in NREM sleep	6 months: Hypsarrhythmia, infantile spasms captured via video electroencephalogram (VEEG)
Epilepsy	Tonic-like seizures with stiffening and staring spells	3 years: Intermittent starring episode; 8 years: Status epilepticus (generalized clonic movement with right eye deviation)	Tonic, spasms and myoclonic generalized seizures	Absences since childhood, about 10 per day; tonic–clonic since 11 years	One episode at 2 years	Yes	Infantile spasms
Well controlled	Yes	No	No	Yes	NA	No	Yes
Treatment	Anti-epileptics × 1 year (Trileptal 5.5 mg bid)	Sultiam, valproic acid	MAD diet at 3:1 ratio, Locasamide, valproate magnesium, clonazepam	Levetiracetam	None	Valproic acid, sultiam, and levetiracetam	Oral prednisolone

Table 1: Summary of epilepsy manifestation including treatment by Hemati et al. (2019) [14].

Symptoms	Individual 3, Petrovski et al. (2016)	Individual 5, Petrovski et al. (2016)	Individual 6, Petrovski et al. (2016)	Individual 7, Petrovski et al. (2016)	Individual 8, Petrovski et al. (2016)	Individual 10, Petrovski et al. (2016)	Individual 11, Petrovski et al. (2016)	Individual 12, Petrovski et al. (2016)	Individual 13, Petrovski et al. (2016)
Mutation (GRCh37; GenBank: NM_002074.4)	chr1: g.1737942A > T	chr1: g.1735987 T > C	chr1: g.1718817C > T	chr1: g.1737953A > C	chr1: g.1735987 T > C	chr1: g.1737942A > G	chr1: g.1737942A > G	chr1: g.1737942A > T	chr1: g.1736004A > G
	c.239 T > A	c.301A > G	c.976G > A	c.228 T > G	c.301A > G	c.239 T > C	c.239 T > C	c.239 T > A	c.284 T > C
	p.Ile80Asn	p.Met101Val	p.Ala326Thr	p.Asp76Glu	p.Met101Val	p.Ile80Thr	p.Ile80Thr	p.Ile80Asn	p.Leu95Pro
EEG	15 months: Generalized subcortical alterations; 3 years: Generalized epileptiform process	7, 10, and 11 months: Modified hypsarrhythmia; 2 years: Normal; 3 years: Multifocal and 2 Hz GSW	14 months: Normal; 5 years: L and R posterior temporal epileptiform activity	Burst suppression	4 years: Normal; 11 years: Diffuse slowing and rare right temporal spikes	2 years: Generalized paroxysmal epileptiform activity, myoclonic seizure with generalized paroxysmal polyspike slow-wave activity	9 years: Multifocal spikes and generalized background slowing	4 years: High amplitude background with occipital slowing, multifocal epileptiform discharges	4 months: Multifocal epileptiform discharges from both posterior quadrants, right temporoparietal sharp waves
Epilepsy	9 months: Generalized epilepsy	Infantile spasms, absence seizures, non-convulsive status epilepticus, focal seizures	1 year: Febrile status epilepticus followed by afebrile focal convulsive seizures and absence and atonic seizures; 14 years: Focal hyperkinetic sleep-related seizures	Hemiclonic seizure associated with hypoglycemia (<20), went into complex partial status	11 years: Onset of tonic–clonic seizures	2 years: Onset of head drops and myoclonic seizures	9 years: Onset of focal seizures	4 years: Onset of focal seizures	4 months: Tonic posturing of the arms and occasional generalized upper-body myoclonus
Well controlled	Unknown	Unknown	Unknown	Unknown	Yes	Unknown	Yes	Unknown	Yes
Treatment	Unknown	Unknown	Unknown	Anti-convulsant therapies	Valproic acid and lamotrigine	Unknown	Onfi and Trileptal	Unknown	Pyridoxal-5-phosphate

Table 1 (continued)

1.3. A92T Variant

To date, the only literature reported patient with the A92T mutation is a girl of Saudi Arabian origin. At the time of diagnosis, she was 2.9 years old. Her phenotype is characterised by GDD, ID, muscular hypotonia, seizures, cerebellar hypoplasia, and ataxia. There are no signs of growth delay, craniosynostosis, abnormal myelination, ophthalmoplegia, nystagmus, chorea, or dystonia. Exome sequencing revealed a *de novo* missense mutation in exon 7 at nucleotide position 274 of *GNB1* (c.274G>A), substituting guanine with adenine, and consequently exchanging alanine for threonine in position 92 of the $G\beta_1$ protein (p.Ala92Thr; highlighted in Figure 3) [1]. As illustrated in Figure 4, alanine is a small, hydrophobic, non-polar amino acid whose side chain is largely non-reactive, yet it may contribute to substrate recognition or specificity. Substitution with threonine introduces a quite reactive, hydrophilic hydroxyl group capable of forming hydrogen bonds with nearby polar substrates. Since Gβ proteins are located intracellularly, this hydroxyl group can also serve as a phosphorylation site for protein kinases. In addition,

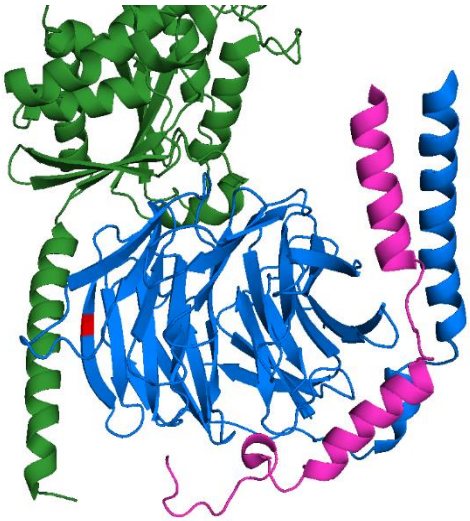

Figure 3: Parts of the $G\alpha_iG\beta_1\gamma_2$ complex (PDB ID 1GP2). Residue 92, located in propeller blade 1, highlighted in red. Green: $G\alpha_i$; blue: $G\beta_1$; pink: $G\gamma_2$.

threonine is one of three Cβ-branched amino acids, resulting in a bulkier side chain that may affect its local structural environment [25].

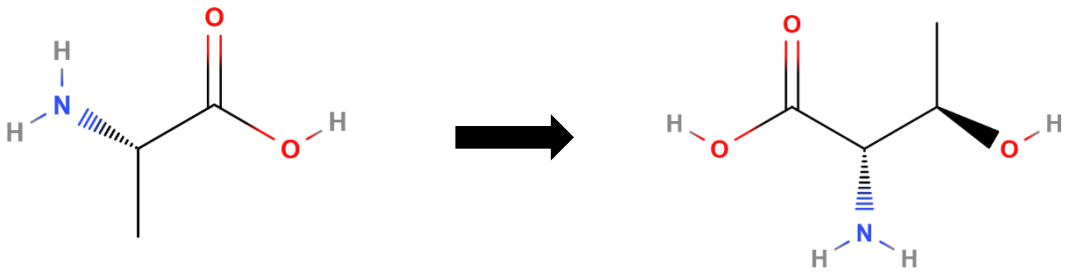

Alanine (A) Threonine (T)

Figure 4: Structural formula of the amino acids alanine (left) and threonine (right). Generated in MolView v2.4.

In a given disease gene, not all protein-altering modifications are to automatically be considered pathogenic. The functional impact of affected signalling molecules can be assessed by their ability to interact with protein partners in the transmission pathway, and to pass on receptor-initiated signals. For the Gβ protein, functionality can be evaluated through its interactions with the other G protein trimer subunits Gα and Gγ, as well as through undergoing receptor-induced rearrangements. In a study published in 2017, Lohmann and colleagues examined changes in these interactions for 10 different *GNB1* missense variants *in vitro* via bioluminescence resonance energy transfer (BRET) [1].

Resonance energy transfer (RET) assays can be used to analyse protein–protein or ligand–protein interaction, recruitment, dissociation, and conformational changes. It is based on non-radiative energy transfer between two chromophores, one labelled as the energy donor and one as the energy acceptor. In BRET, a luminescent luciferase-based donor and a fluorescent acceptor are tagged to the interaction partners of interest. When the proteins align, the acceptor is excited and a signal can be measured in a photometer [26, 27]. Lohmann et al. investigated the $G\beta_1\gamma_7$ dimer formation, heterotrimer assembly with $G\alpha_{olf}$, and mediation of dopamine receptor D1R signalling through binding of GRK3. They tagged each of the $G\beta_1\gamma_7$ dimer subunits with a non-fluorescent fragment of Venus, a yellow fluorescent protein, and GRK3 with Nluc, an engineered nanoluciferase. That way it was possible for them to first measure $G\beta_1\gamma_7$ dimer formation using bimolecular fluorescence complementation (BiFC), then measuring BRET ratio and response when in close proximity of Nluc-tagged GRK3 (Figure 5A and C) [1].

Mutations A92T showed a significantly elevated basal BRET ratio (Figure 5B), implying weakened association between $G\beta_1\gamma_7$ and $G\alpha_{olf}$, while maintaining interaction with GRK3. This leads to the assumption that, in this specific instance, A92T is a constitutively active variant and may exhibit gain-of-function (GoF) characteristics similar to those observed in oncogenic Gβ mutations. However, the agonist-induced BRET response was

significantly lower in amplitude compared with the wild type (Figure 5D), suggesting a decreased capacity to mediate receptor signalling due to the higher basal activity. Contrary to the basal BRET results, this observation insinuates a loss of function (LoF) – at least regarding the transduction of neurotransmitter signals – which might be the origin for its disease-causing effect.

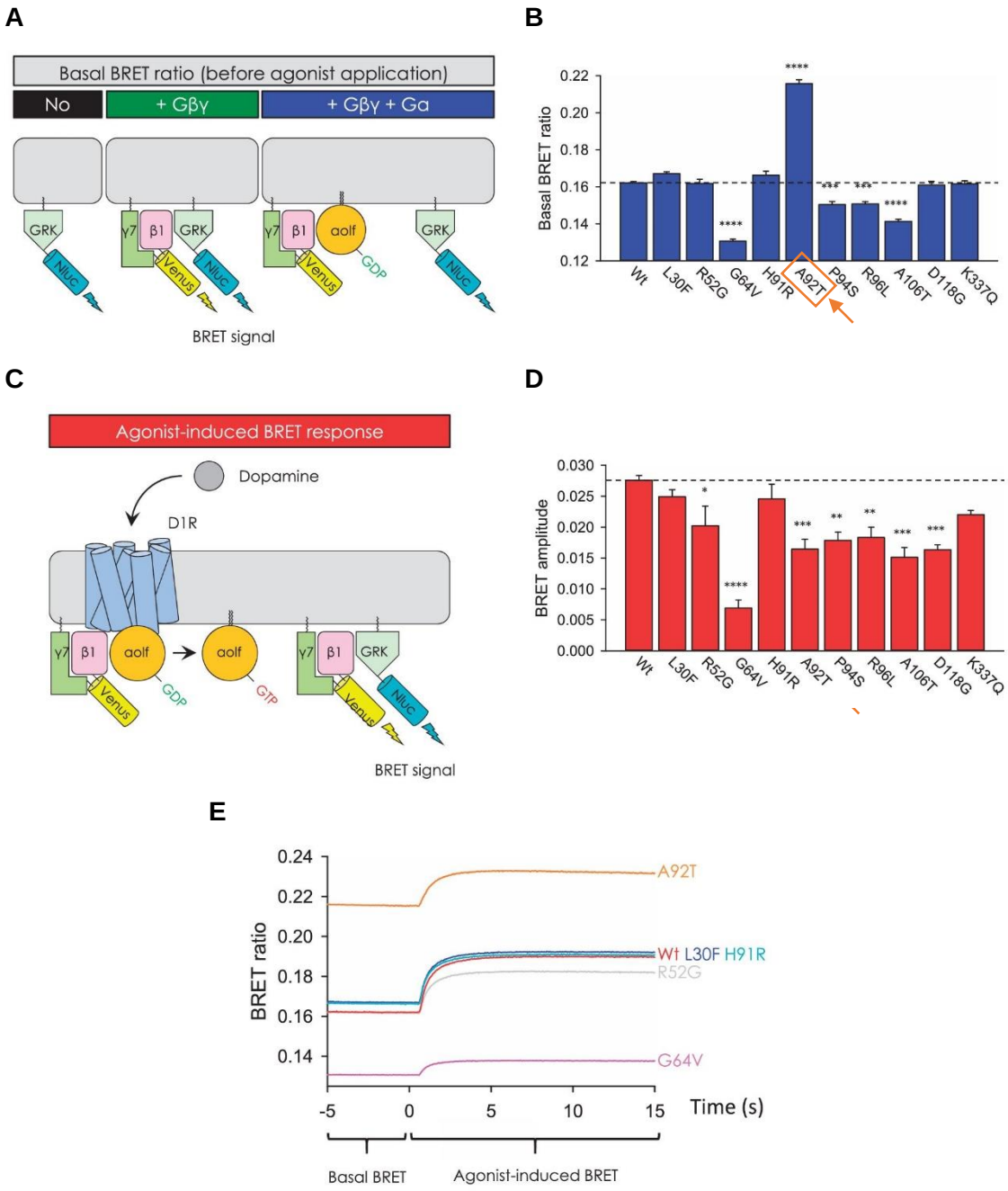

Figure 5: Results BRET assay, adapted figure by Lohmann et al. [1]. A) Schematic representation of basal BRET ratio assessment. B) Results basal BRET ratio, A92T highlighted. C) Schematic representation of Agonist-induced BRET response. D) Results BRET amplitude, A92T highlighted. E) Representation of D1R-G_{olf} signalling before and after agonist application.

However, these *in vitro* findings might not fully relate to *in vivo* conditions, especially regarding LoF and GoF observations, as only one specific heterotrimer constellation and a single signal transduction pathway were tested [1].

1.4. MD Simulation & Calculation of Free Energy Changes

1.4.1. Principle

Free energy is fundamental to both thermodynamics and kinetics, making the precise prediction of differences in free energy after amino acid mutation a main objective of computer-aided molecular design. Knowledge about the free energy surface of a system enables the understanding of biophysical processes such as protein folding, ligand binding, and protein–protein associations. Various computational methods have been developed for assessing free energy changes associated with differences in stability and binding affinity between wild-type and mutant proteins, among them methods that build on molecular dynamics (MD) simulations [28].

MD simulations are a useful tool for studying the nature of classical many-particle systems. They were developed in the mid-1950s by Alder and Wainwright and allow for systematic analysis of structural, dynamical, and thermodynamic properties that would be difficult to obtain otherwise. Instead of attempting to measure the behaviour of such systems directly, MD simulations follow the natural time evolution of the system as dictated by Newton's equations of motion. From the resulting trajectories, we can then approximate the relevant quantity of interest by averaging them over sufficiently long periods of time. Physical and numerical measurements are very distinct from one another. In physical measurements, we utilise probes such as pressure gauges or thermometers to gather information, whereas in simulations, the values of the observed variables are derived from all the particles' positions and momenta using statistical mechanics. It is important to recognize that not every value computed in a simulation can be directly compared to experimental measurements and predicted properties always belong to a *model* system [29]. Both simulations and experiments have advantages and disadvantages, providing information not obtainable through the other. Therefore, MD simulations are a great addition to conventional experiments and allow assessment of whether theoretical models are consistent with experimental results [30].

1.4.2. Theory

This chapter is focused on the central concepts of physics-based computer simulations. In solution, a polypeptide chain can exist in well-defined secondary and tertiary structures as well as several disordered configurations. The collection of disordered conformations is commonly referred to as the unfolded state (state A), whereas the ordered conformations constitute the folded state (state B). Sampling the entire conformation

landscape of a protein is rarely feasible in practice, and focus is generally placed on differences in free energy (ΔG) rather than on absolute free energies. ΔG directly reflects the ratio of probabilities of the system occupying state A relative to state B [28].

$$\frac{p_A}{p_B} = \frac{e^{-\beta G_A}}{e^{-\beta\, G_B}} = e^{-\beta\,(G_A - G_B)} \qquad\qquad \Delta G = G_A - G_B = -k_B T \ln \frac{p_A}{p_B}$$

G resembles the free energy of a system with a fixed number of particles and isothermal–isobaric conditions. $\beta = 1/k_B T$, where k_B is the Boltzmann constant and T the absolute temperature. ΔG sets the maximum possible work of a closed system, achievable only under reversible conditions. Real processes, however, occur in finite time intervals τ, cause heat dissipation, and are thus irreversible. Consequently, the work performed during a process is on average equal to or greater than ΔG, in line with the second law of thermodynamics [28].

$$\langle W(\tau) \rangle \geq \Delta G$$

For $\tau \to \infty$, $\langle W(\tau) \rangle$ is equal to ΔG. For finite τ, the difference between $\langle W(\tau) \rangle$ and ΔG is dependent on the thermodynamic path chosen. The work done on a system can be calculated by integrating the energy costs required to change it [28].

$$W(\tau) = \int_{\lambda=0}^{\lambda=1} \frac{\partial \mathcal{H}(x, v, \lambda)}{\partial \lambda}\, d\lambda$$

λ is a parameter driving a non-equilibrium process along a specific path. At $\lambda = 0$, the process begins, and at $\lambda = 1$, the process ends. $\mathcal{H}$ is the Hamilton operator of the system and is dependent on λ as well as the phase space coordinates x and the velocities v of the system. Based on these considerations ΔG can be estimated using both equilibrium and non-equilibrium simulations. Classical approaches such as free energy perturbation (FEP) and thermodynamic integration (TI) rely on equilibrium ensemble averages, while more recent methods, based on Jarzynski's equality and the Crooks Fluctuation Theorem (CFT), enable calculations from non-equilibrium work distributions. Jarzynski's equality establishes a connection between the average work performed in a non-equilibrium process and the equilibrium free energy difference [28].

$$\langle e^{-\beta W(\tau)} \rangle = e^{-\beta \Delta G}$$

However, Jarzynski's equality only accounts for one directional transitions, whereas the CFT considers both forward and reverse work distributions [28].

$$\frac{P_f(W)}{P_r(-W)} = e^{\beta(W-\Delta G)}$$

$P_f(W)$ and $P_r(-W)$ are the normalized probability distribution for the respective forward and reverse work values. Based on this equation, ΔG can be assessed [28].

$$\widehat{\Delta G} = W + k_B T \ln \frac{P_f(W)}{P_r(-W)}$$

$\widehat{\Delta G} = W$ describes the intersection of the work distributions. This approach faces limitations, however, they can be partially mitigated by using ΔG estimators. For example, the Bennett acceptance ratio (BAR) directly combines information from forward and reverse distributions to obtain an ideal estimate of ΔG [28].

$$\sum_{i=1}^{N_f} \frac{1}{1 + \frac{N_f}{N_r} e^{\beta(W_i - \widehat{\Delta G})}} = \sum_{j=1}^{N_r} \frac{1}{1 + \frac{N_r}{N_f} e^{-\beta(W_j - \widehat{\Delta G})}}$$

In order to obtain ΔG, we have to characterise the initial and final states as well as the connecting path. For calculation of the folding free energy of a protein, we define the unfolded protein as the initial state, and the folded protein as the final state. In principle, the protein can be unfolded through pulling its termini apart and measuring the required work, but such disturbances require extensive calculating to achieve convergence. A more efficient strategy for studying the change in folding free energy upon protein mutation ($\Delta\Delta G_{Folding}$) is to build a thermodynamic cycle with alchemical, that is non-physical, transformations involving smaller perturbations, and therefore easier convergence (illustrated in Figure 6). As a result, it is computationally more practical to mutate a wild-type protein into its variant than to simulate the folding and unfolding of both. Since G is a state function, the chosen pathway does not affect the final result [28].

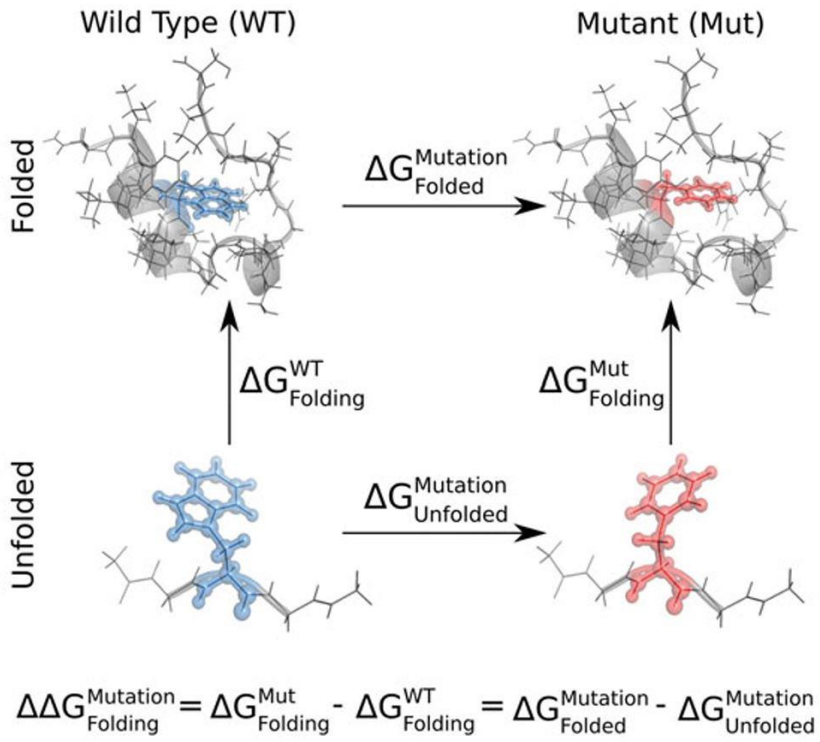

Figure 6: Schematic representation of a thermodynamic cycle for calculating changes in free energy of protein folding in mutations ($\Delta\Delta G^{Mutation}_{Folding}$) [28].

2. Objective

Since *GNB1*-E is a rare condition, little is known about the exact mechanism, how these $G\beta_1$ subunit mutations disrupt cellular function and cause disease. In order to better understand the structural mechanisms of the pathogenic A92T variant, MD simulations were conducted. Considering the significantly different BRET signals between the wild type and the mutation reported by Lohmann et al. (2017) [1], there may be alterations in the binding behaviour of $G\beta_1$. Building on the results of the master's thesis of Elbashat (2025), which show no significant effect of the A92T mutation on $G\beta_1\gamma_2$ dimer stability [31], the present work aims to investigate possible alterations in the interaction of the $\beta_1\gamma_2$ subunit with $G\alpha_i$ and GRK2. A deeper understanding of the effects at the molecular level helps define the pathophysiology of *GNB1*-E as well as pinpoint where in the various signalling pathways the problems first arise. This knowledge lays the foundation for finding treatment options for affected individuals, for example GIRK-Inhibitors for patients affected by certain types of seizures [32], or small molecules able to change protein–protein interactions and therefore normalise GPCR signalling.

3. Materials and Methods

3.1. Simulation Preparation

MD simulations were carried out using GROMACS (version 2022.3) [33] running on Ubuntu Linux (version 20.04.6).

The protein structures for the MD simulations were retrieved from the Research Collaboratory for Structural Bioinformatics Protein Data Bank (RCSB PDB) and prepared using CHARMM-GUI [34]. For the $G\beta_1\gamma_2$ system, the dimer was extracted from structure 4KFM [35], which is the crystal structure of the mammalian GIRK2 channel in complex with four $G\beta_1\gamma_2$ subunits. PDB structure 1GP2 [36] was gathered for the $G\alpha_iG\beta_1\gamma_2$ heterotrimer. Lastly, structure 1OMW [37] was used for the $G\beta_1\gamma_2$GRK2 complex.

The force field implemented in the simulations was Amber99SB*ILDN [38], and the calculations were performed in a protein-in-water system (TIP3P). For hybrid topology and tripeptide system generation, the pmx webserver was used [39]. The tripeptides – in this case GAG and GTG, respectively – are an approximation for the unfolded state of the protein, as the unfolded full-length protein is difficult to simulate.

3.2. Protocol

The pipeline for calculating free energy begins with energy minimisation in order for the system to start in a stable, low-energy state. This is followed by NVT (constant number, volume, temperature) and NPT (constant number, pressure, temperature) equilibration for 100 ps. Production MD is executed for 10 ns, of which the first 2 ns are excluded. The last 8 ns are used to create 100 equally spaced frames (1 frame per 80 ps) as a basis for the subsequent non-equilibrium transitions, running 50 to 200 ps. The work values required for shifting the wild type into the mutant and vice versa are collected and the Crooks fluctuation theorem is used for determining the free energy difference between the two states [40]. Estimations are made using the Bennett acceptance ratio (BAR) [41].

This protocol was repeated five times for the tripeptide and the $G\beta_1\gamma_2$GRK2 complex, as well as six times for the $G\alpha_iG\beta_1\gamma_2$ heterotrimer. In order to calculate the root mean square deviation (RMSD) of the $G\alpha_i$ chain of the G protein and the root mean square fluctuation (RMSF) of $G\beta_1$, run 6 was extended to 250 ns.

Using the same extended run, the energy impact of the mutation was calculated for neighbouring residues of $G\alpha_i$ as well as $G\beta_1$ itself, and the results were compared to energy interactions of the wild type.

4. Results

In this thesis, the impact of the A92T mutation on the $G\beta_1\gamma_2$ interaction with $G\alpha_i$ as well as GRK2 was examined. In order to investigate the potential effects, MD simulations for several structures were conducted, including the $G\alpha_iG\beta_1\gamma_2$ heterotrimer, the $G\beta_1\gamma_2$GRK2 complex, and a tripeptide carrying the mutation. Free energy changes upon amino acid mutation (ΔΔG) were calculated, and following an extended MD run, RMSD for $G\alpha_i$ and RMSF for $G\beta_1$ were determined. The results are summarised below and will be discussed further in the discussion section.

4.1. Tripeptide

Figure 7 displays the work profiles obtained from non-equilibrium simulations of the A2T tripeptide model for all five runs. Values of the forward transitions are depicted in green, backward values are presented in blue. Since the simulations have been performed under isothermal conditions, the estimated free energy change of the respective systems (ΔG) correlates to work being done. ΔG values were calculated using the BAR method. On the left side of the figures, the work values are plotted against the number of snapshots taken. The right side shows histograms of the values' distributions as well as the estimated ΔG, indicated by the black dashed line. The mean ΔG value of the five tripeptide simulation runs is later used to calculate the ΔΔG values of the examined proteins.

Figure 7: Free energy calculations for the A2T tripeptide model. Left: work values for forward and backward transitions. Right: corresponding work distributions and estimated ΔG.

Run 1	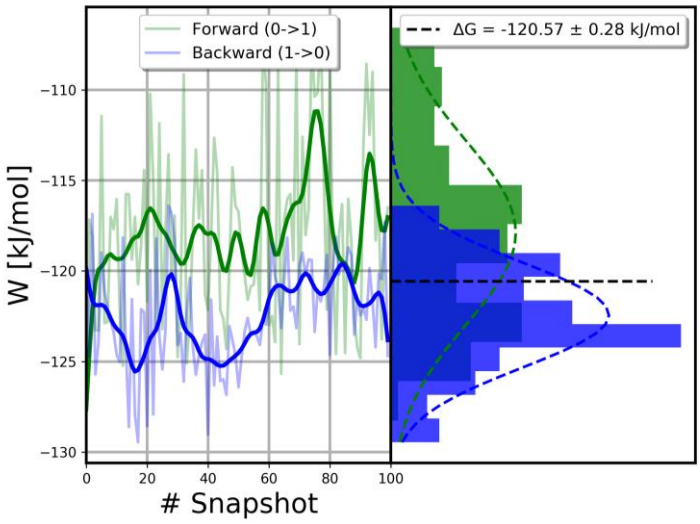

Run 2	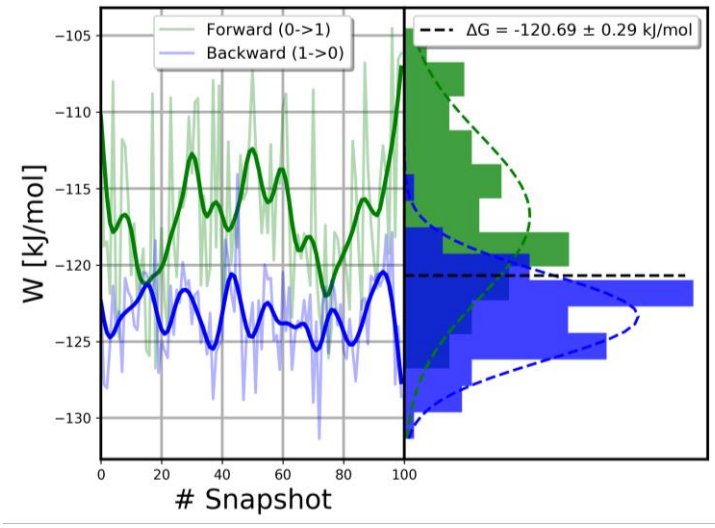
Run 3	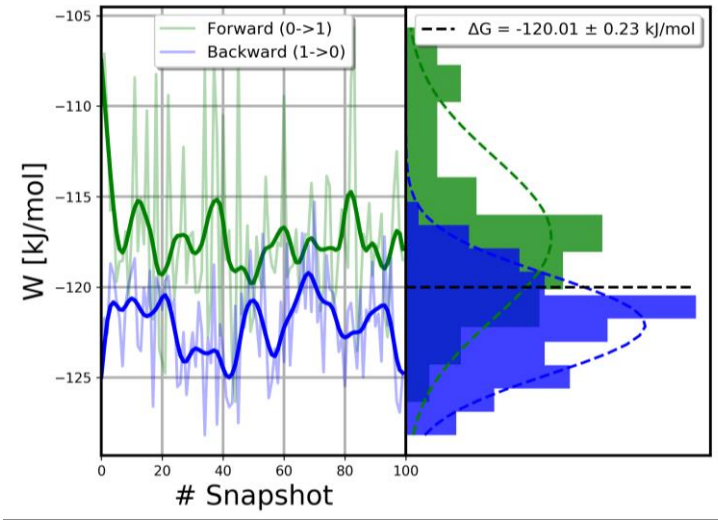
Run 4	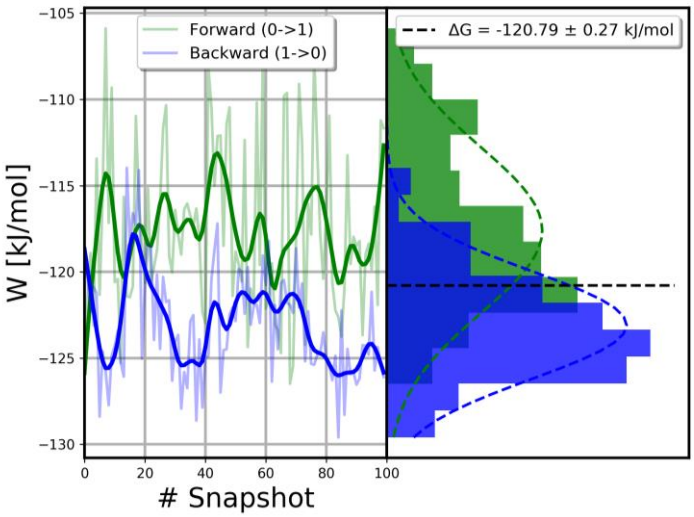

Figure 7 (continued)

Run 5	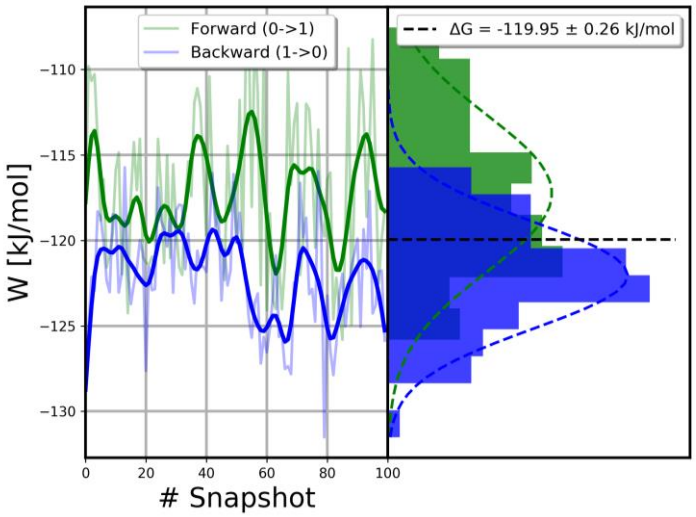

Figure 7 (continued)

The mean ΔG value was determined by averaging the results of the five runs.

$$\Delta G^{average}_{tripeptide} = \frac{-120.57+(-120.69)+(-120.01)+(-120.79)+(-119.95)}{5} = -120.40\ kJ/mol$$

4.2. GαᵢGβ₁γ₂

Figure 8 shows the results acquired by non-equilibrium simulations of the A92T mutated GαᵢGβ₁γ₂ complex for all six runs. The depiction is equal to the one explained in chapter 4.1.

Figure 8: Free energy calculations for the A92T mutated GαᵢGβ₁γ₂ complex. Left: work values for forward and backward transitions. Right: corresponding work distributions and estimated ΔG.

Run 1	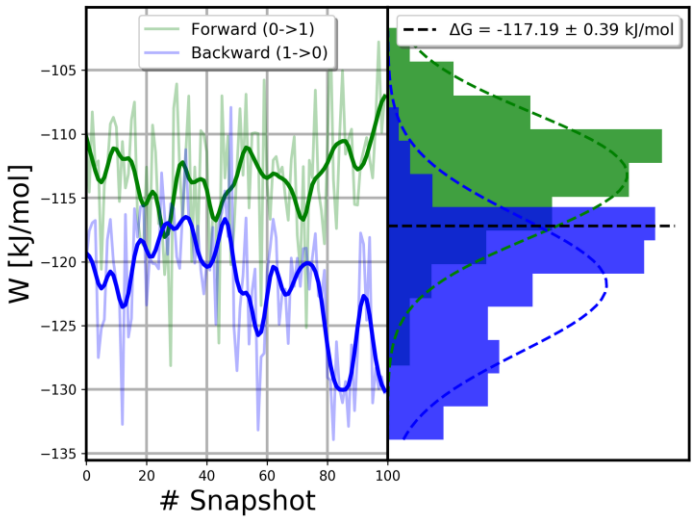

Run 2	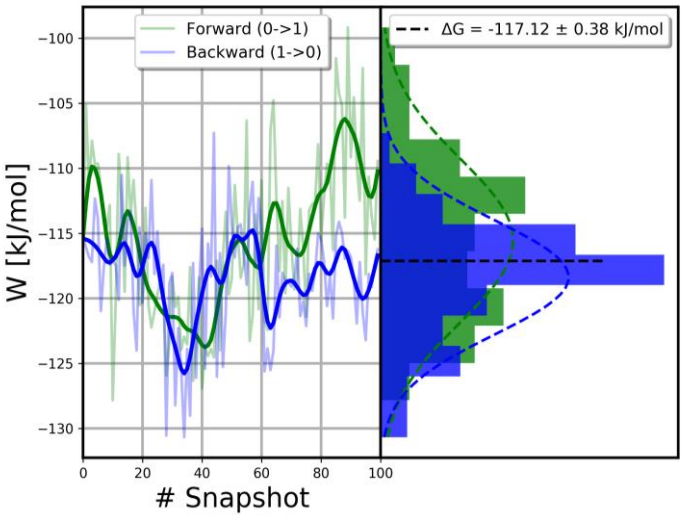
Run 3	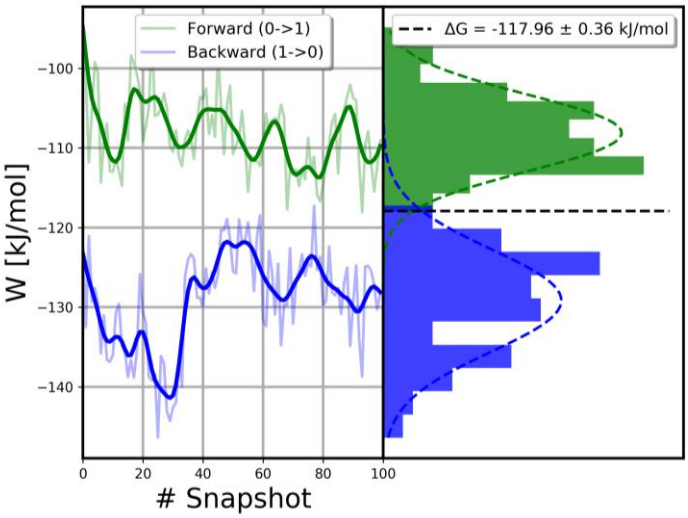
Run 4	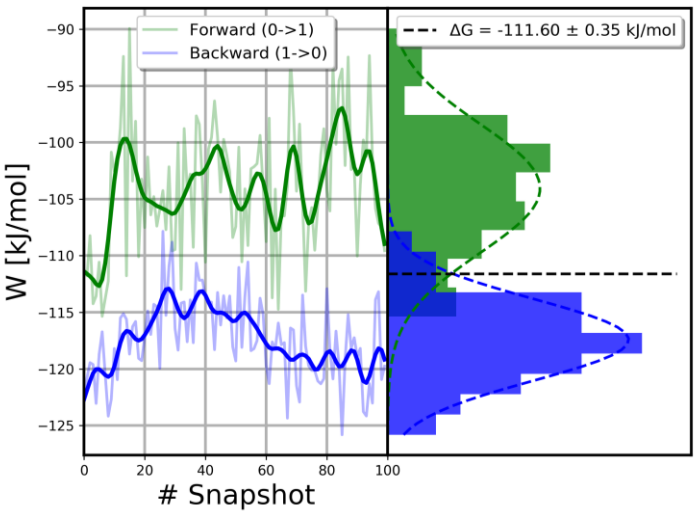

Figure 8 (continued)

Run 5	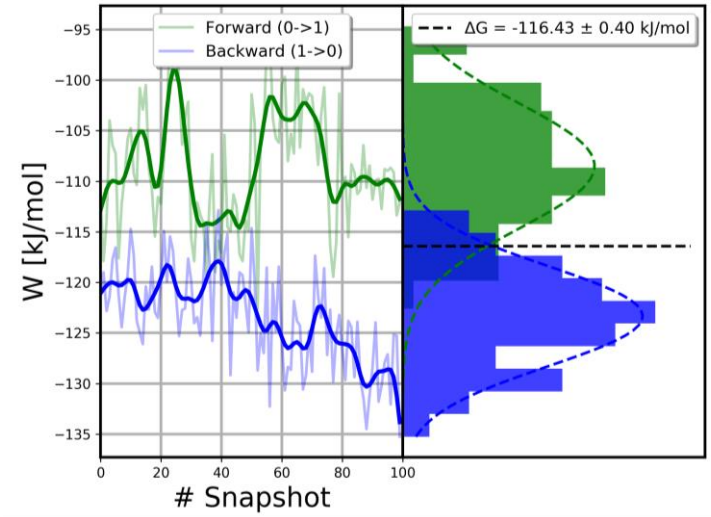
Run 6	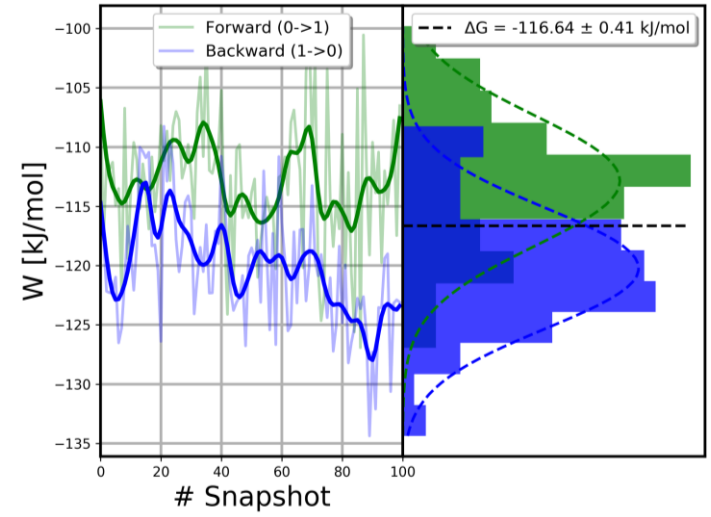

Figure 8 (continued)

4.3. Gβ$_1$γ$_2$GRK2

Figure 9 presents the results acquired by non-equilibrium simulations of the A92T mutated Gβ$_1$γ$_2$GRK2 complex for all five runs. The depiction is equal to the one explained in chapter 4.1.

Figure 9: Free energy calculations for the A92T mutated Gβ$_1$γ$_2$GRK2 complex. Left: work values for forward and backward transitions. Right: corresponding work distributions and estimated ΔG.

Run 1	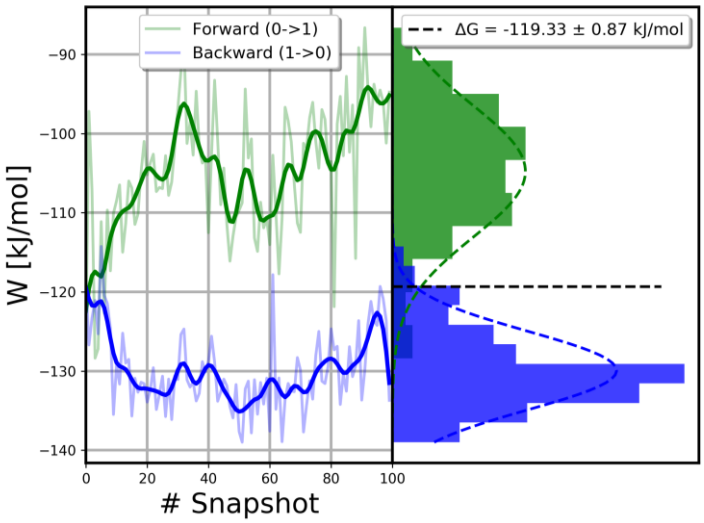
Run 2	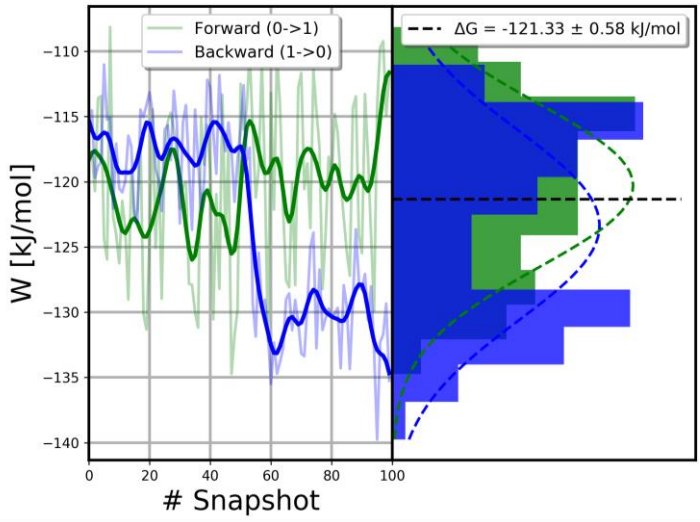
Run 3	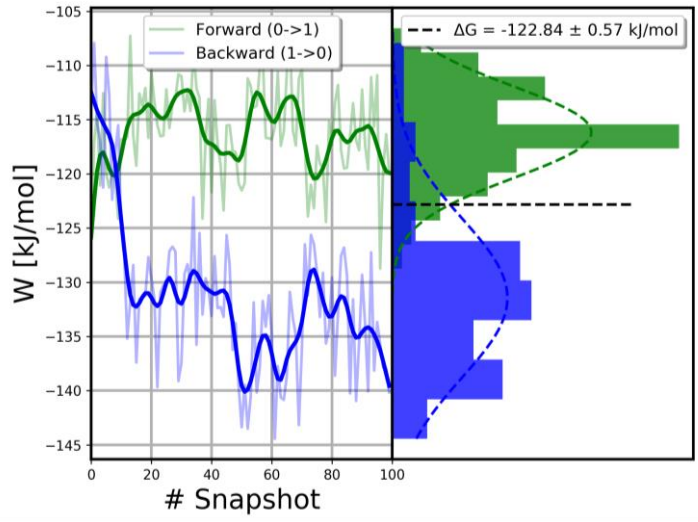

Run 4	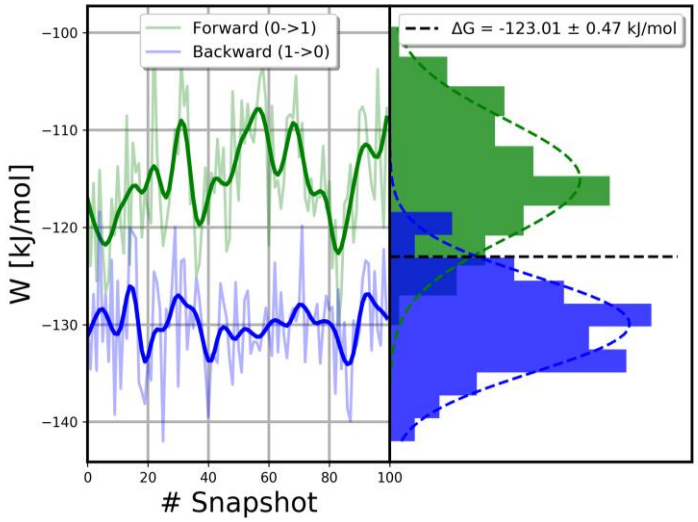
Run 5	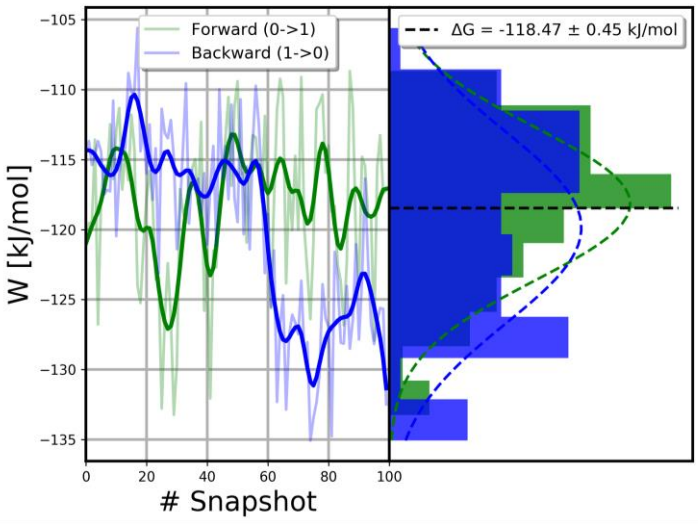

Figure 9 (continued)

4.4. ΔΔG Calculations

By applying the following formula provided by Aldeghi et al. (2019), ΔΔG values were calculated and are summarised in Table 2 and Table 3:

$$\Delta\Delta G_{Folding}^{Mutation} = \Delta G_{Folded}^{Mutation} - \Delta G_{Unfolded}^{Mutation} \quad [28]$$

Since the tripeptide system was previously established to represent the unfolded protein state, ΔG_{tripep}^{avg} calculated in chapter 4.1 was subtracted from the respective protein simulation results in order to obtain ΔΔG values. Positive values indicate a destabilising effect of the mutation on the complex, negative values a stabilising effect. Data suggest a mean unsigned error of 4 kJ/mol in the predictions due to limited sampling size and force-field limitations.

Run	ΔΔG (kJ/mol)
1	3.21
2	3.28
3	2.44
4	8.80
5	3.97
6	3.76
$\Delta\Delta G^{avg}_{G\alpha i\beta 1\gamma 2} = 4.25\ kJ/mol$	

Table 2: Calculated ΔΔG values for the $G\alpha_iG\beta_1\gamma_2$ complex.

Run	ΔΔG (kJ/mol)
1	1.07
2	-0.93
3	-2.44
4	-2.61
5	1.93
$\Delta\Delta G^{avg}_{G\beta 1\gamma 2GRK2} = -0.59\ kJ/mol$	

Table 3: Calculated ΔΔG values for the $G\beta_1\gamma_2$GRK2 complex.

Figure 10 visualises the average ΔΔG values and standard deviations obtained for all three complexes: $G\beta_1\gamma_2$, $G\alpha_iG\beta_1\gamma_2$, and $G\beta_1\gamma_2$GRK2. The average difference in energy states during the transformation of $G\beta_1\gamma_2$ into $G\alpha_iG\beta_1\gamma_2$ for the A92T mutant differs by 4.57 kJ/mol compared to the wild type. The average difference in energy states for the $G\beta_1\gamma_2$GRK2 into $G\alpha_iG\beta_1\gamma_2$ transformation differs by 4.84 kJ/mol for this variant. Thus, in the case of the A92T mutation, the stability of the $G\alpha_iG\beta_1\gamma_2$ complex is reduced more than the average kinetic energy of the particles (3.9 kJ/mol) at a temperature of 310 K compared to the complexes $G\beta_1\gamma_2$ and $G\beta_1\gamma_2$GRK2.

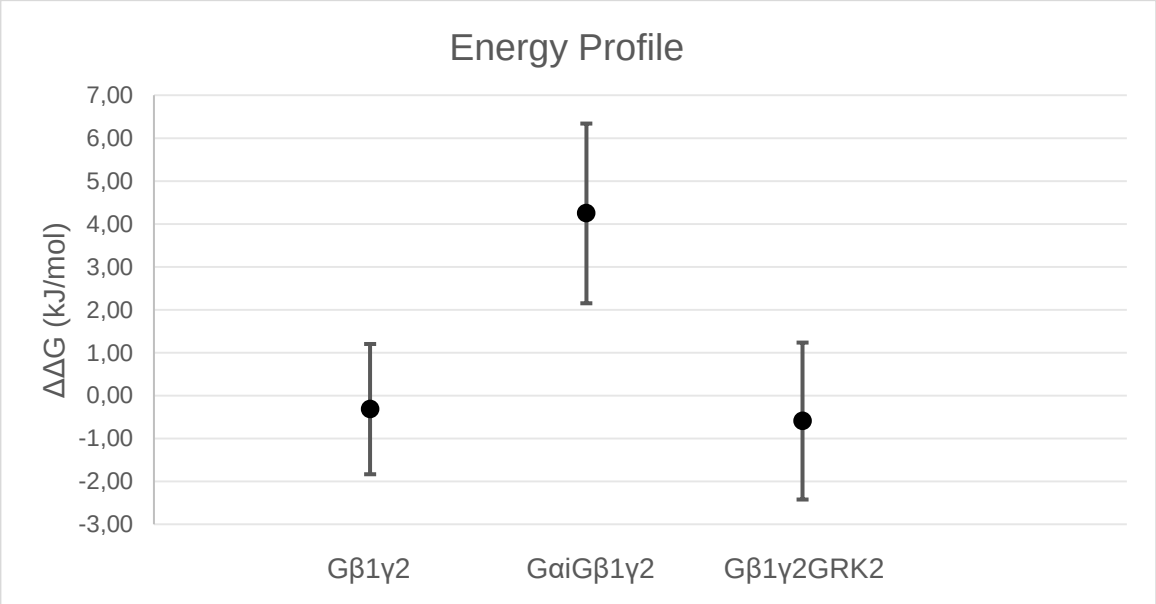

Figure 10: Energy profiles compared. Data for Gβ1γ2 obtained from Elbashat (2025) [31]. Dots: average ΔΔG; error bars: standard deviation.

4.5. Root Mean Square Deviation (RMSD)

To further evaluate the impact of the A92T variant on the $G\alpha_iG\beta_1\gamma_2$ heterotrimer, RMSD values were computed for the wild type as well as the mutant over a 250 ns extended simulation run. This measurement indicates whether a protein is stable and similar to the experimental structure. Figure 11 shows the RMSD values obtained for the $G\alpha_i$ subunit when in complex with wild-type compared to mutant $G\beta_1$. RMSD values for the wild-type system fluctuate around 0.35 nm, while mutant values are around 0.45 nm.

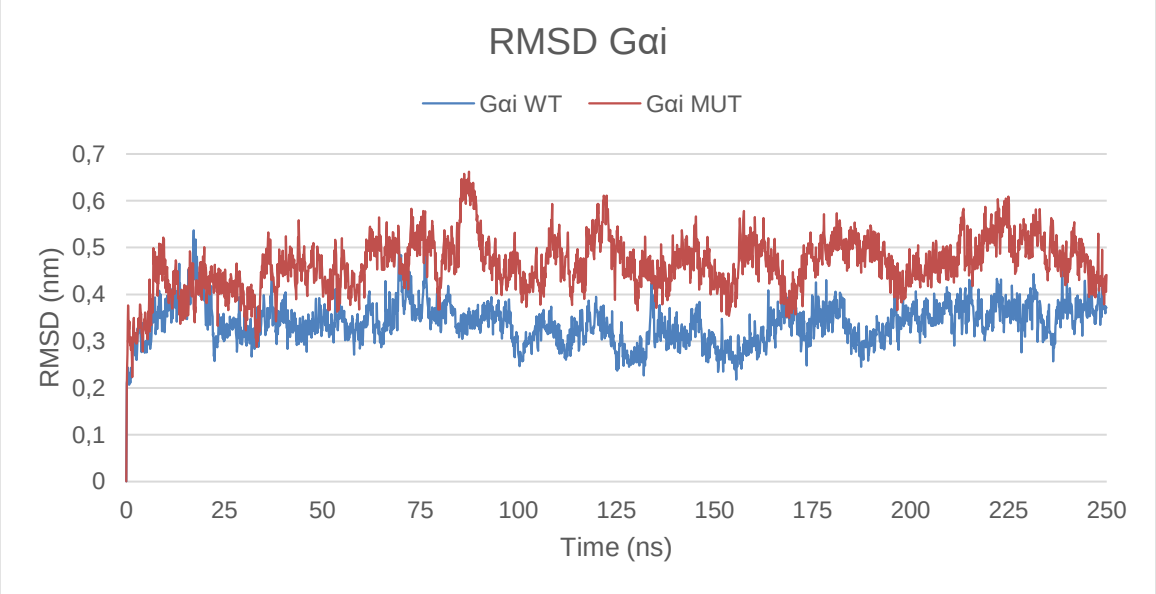

Figure 11: RMSD of the $G\alpha_i$ subunit during a 250 ns MD simulation. Blue: wild-type system; red: mutant system.

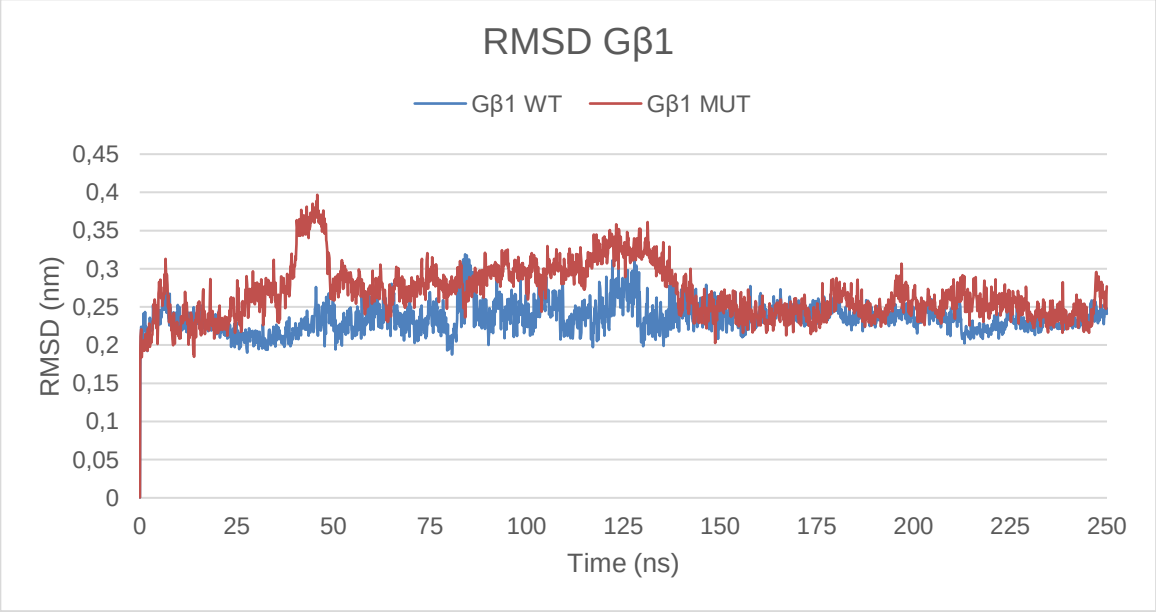

Figure 12: RMSD of the $G\beta_1$ subunit during a 250 ns MD simulation. Blue: wild-type system; red: mutant system.

Figure 12 depicts the RMSD values calculated for the $G\beta_1$ subunit itself. For the wild type, RMSD values fluctuate around 0.25 nm, while the mutated protein graph shows a peak at about 40-50 ns and an overall higher average deviation of around 0.3 nm until approximately 140 ns of simulation. After that, RMSD values are similar for both variants.

4.6. Root Mean Square Fluctuation (RMSF)

RMSF was assessed for the wild-type as well as the mutant $G\beta_1$ subunit during the extended 250 ns MD simulation. Residue fluctuation values highlight regions of the protein that remain flexible within the structure, even as the overall conformation reaches stability over the course of the simulation. Figure 13 illustrates the results received for the Gβ chain of the complex. The calculated RMSF values show no significant differences between the wild-type and the mutated protein.

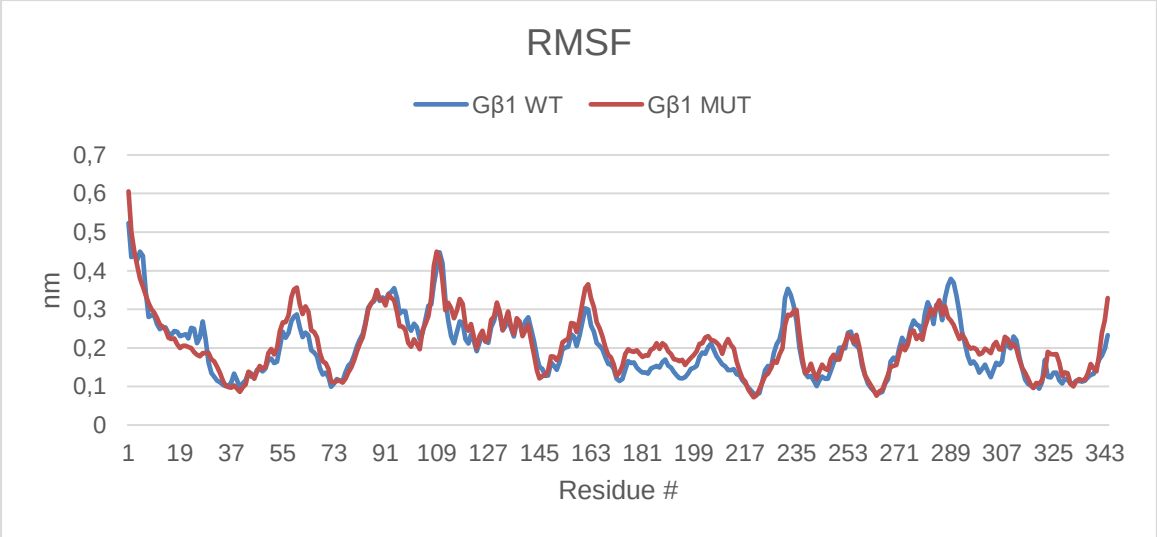

Figure 13: RMSF of the $G\beta_1$ subunit during a 250 ns MD simulation. Blue: wild type; red: mutant.

4.7. Residue Energy Analysis

In this step, the energy impact of residue 92 on surrounding amino acids was calculated for both the wild type and the mutation using data from the extended MD run 6. Firstly, data for $G\alpha_i$ was computed, followed by $G\beta_1$. Interaction data was retrieved in form of non-bonded interactions (electrostatic and non-electrostatic), Coulomb energy (electrostatic potential), and Lennard-Jones potential (non-electrostatic energy).

Additionally, non-bonded interactions between A92T and water was calculated (Figure 14). This figure suggests considerably higher interactions of the mutated $G\beta_1$ protein with water than the wild type. From approximately 20 ns to 55 ns of simulation time, the interaction energy increases towards zero, indicating a transient loss of strong interactions. This may be due to the threonine side chain adopting an inward-oriented or shielded conformation within the protein matrix.

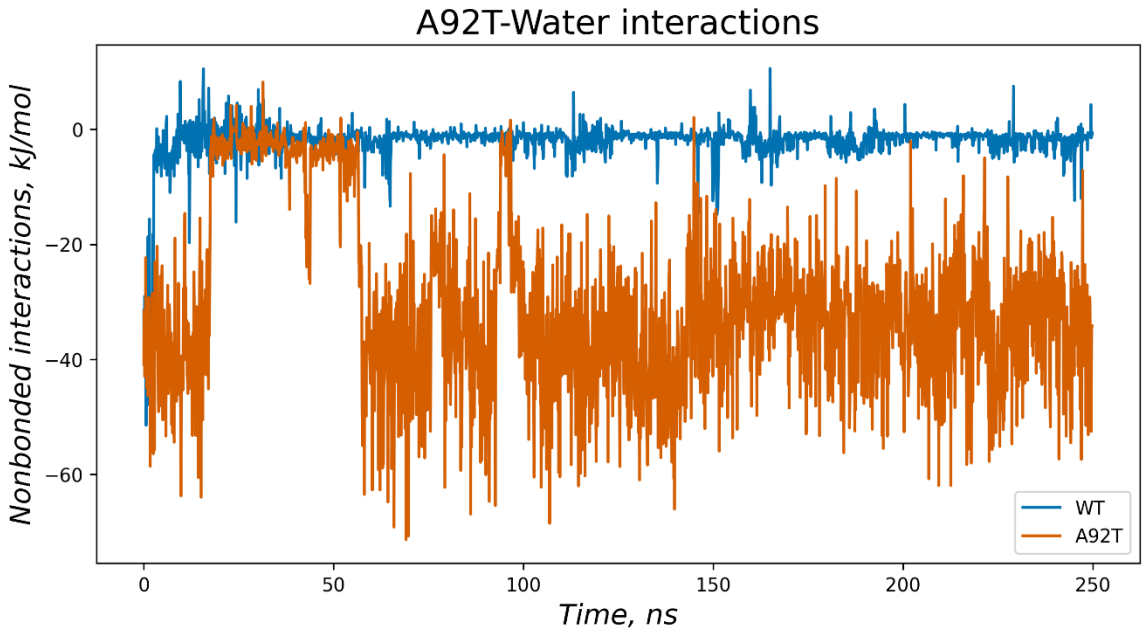

Figure 14: Non-bonded interactions between A92T and water, computed over 250 ns MD simulation time. Blue: wild type, orange: mutant.

4.7.1. Gαᵢ

Figures 15-17 show the energy impact that A92T exerts on the Gαᵢ subunit. Overall, the energy values are similar throughout the different interaction types. Residue 16 exhibits the strongest non-bonded interaction and Lennard-Jones energy.

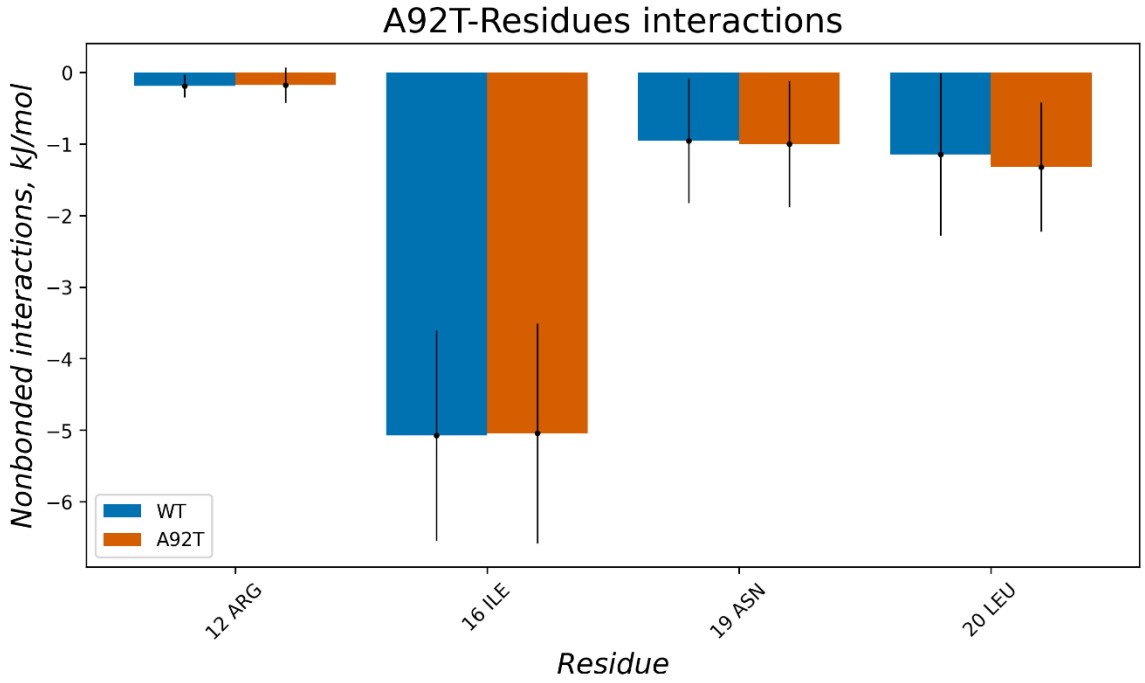

Figure 15: Non-bonded interactions between A92T and Gαᵢ, computed over 250 ns MD simulation time. Blue: wild type, orange: mutant.

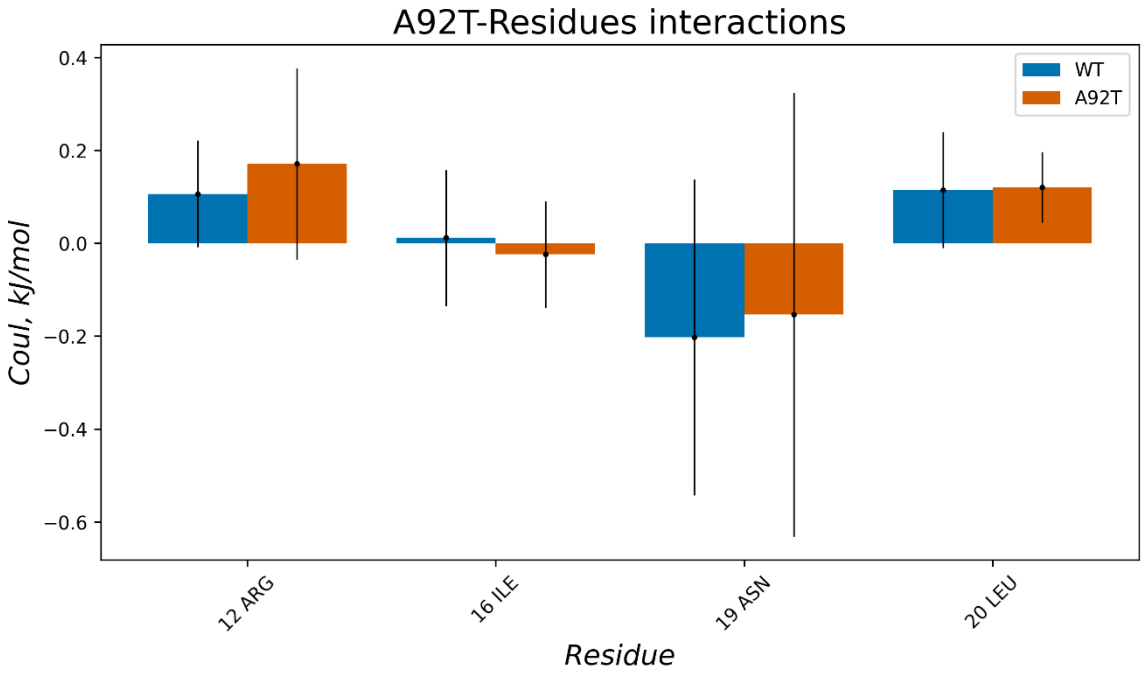

Figure 16: Coulomb energy for A92T and Gα$_i$, computed over 250 ns MD simulation time. Blue: wild type, orange: mutant.

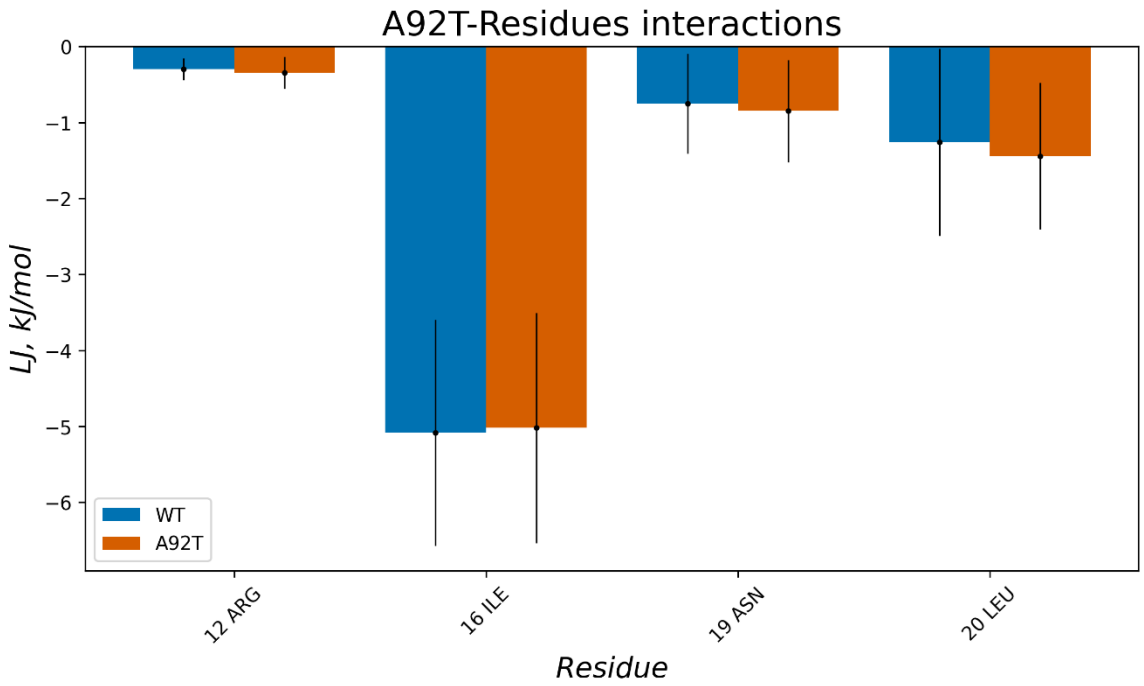

Figure 17: Lennard-Jones energy for A92T and Gα$_i$, computed over 250 ns MD simulation time. Blue: wild type, orange: mutant.

4.7.2. $G\beta_1$

Figures 18-20 show the energetic effects that A92T has on $G\beta_1$. In this chain, more differences in energy values emerge than in $G\alpha_i$, especially from residue 128 upwards.

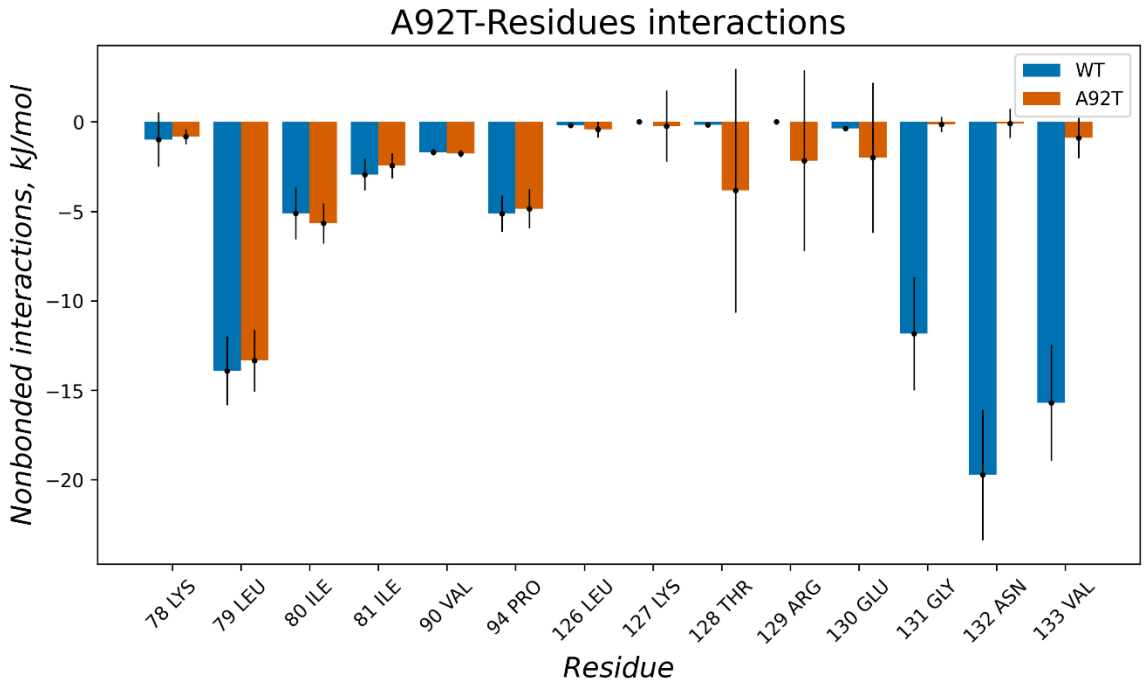

Figure 18: Non-bonded interactions between A92T and $G\beta_1$, computed over 250 ns MD simulation time. Blue: wild type, orange: mutant.

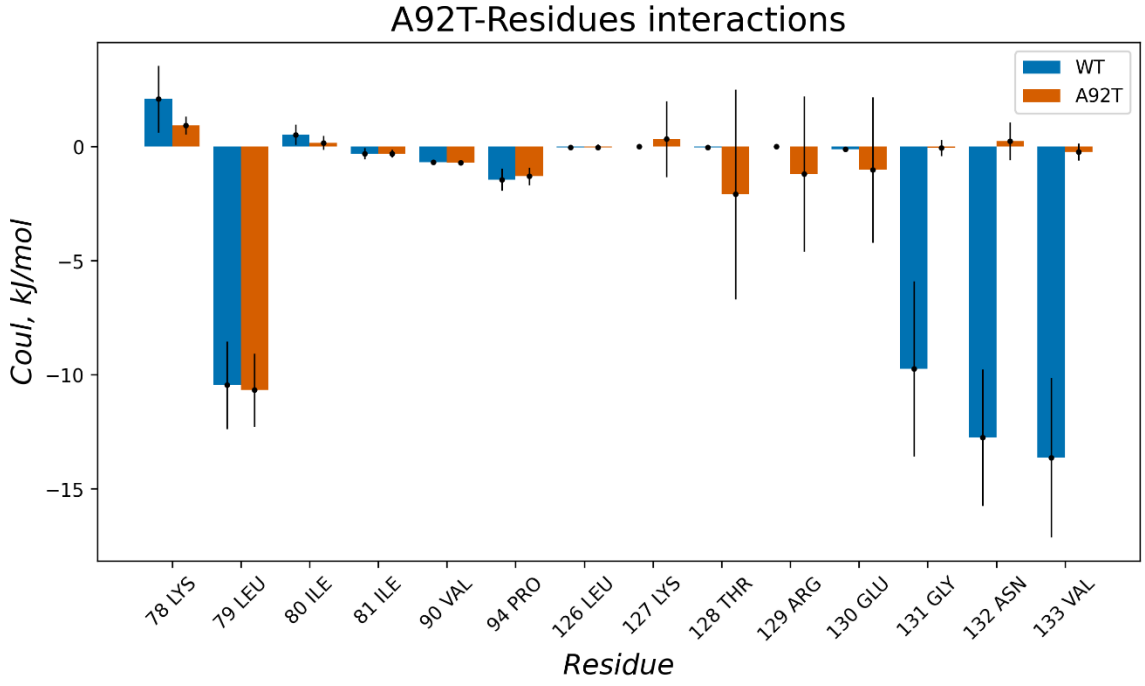

Figure 19: Coulomb energy for A92T and $G\beta_1$, computed over 250 ns MD simulation time. Blue: wild type, orange: mutant.

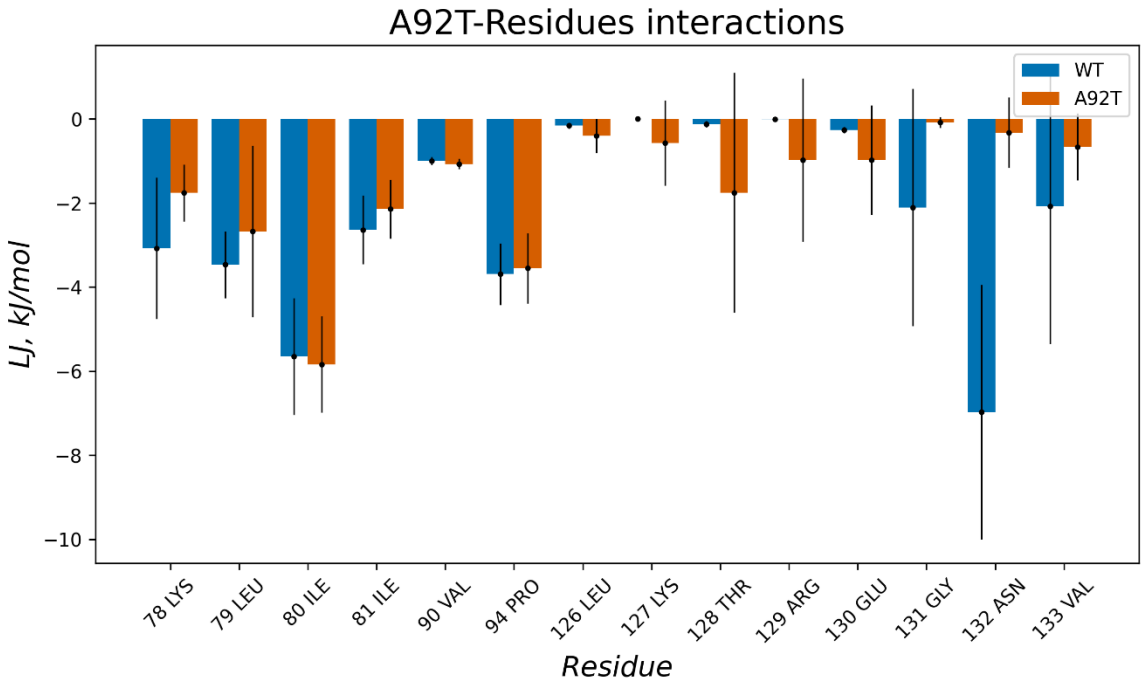

Figure 20: Lennard-Jones energy for A92T and Gβ₁, computed over 250 ns MD simulation time. Blue: wild type, orange: mutant.

Residue 80 displays strong energy values for both the wild type and the mutant for all three interaction types measured. For residues 127 to 130, the wild type shows little to no interactions, whereas the mutant exhibits weak interaction energies. The most visible change in energy interactions happens at residues 131 to 133, where to some extent the wild-type protein has strong effects, however, the mutant shows almost none.

4.7.3. GRK2

Figure 21 illustrates residues in wild-type Gβ₁ as well as GRK2 that exert non-bonded interactions to a certain extent. The values were calculated in the Amber99SB*ILDN force field over 10 ns MD simulation time in Anna Weinzinger's Lab by PhD student Ilia Steshin, and are available on GitLab [42]. Since residue 92 is not shown, it can be assumed there are neither stabilising nor destabilising interactions occurring between A92 and GRK2. As this does not suggest that A92T plays an important role in the disease mechanism, no further detailed investigations were conducted for this protein.

Nevertheless, the figure points out interesting data relevant for future work, for example how the L95P mutation known to be disease-causing would alter the stabilising effect residue 95 has on the $G\beta_1\gamma_2$GRK2 complex.

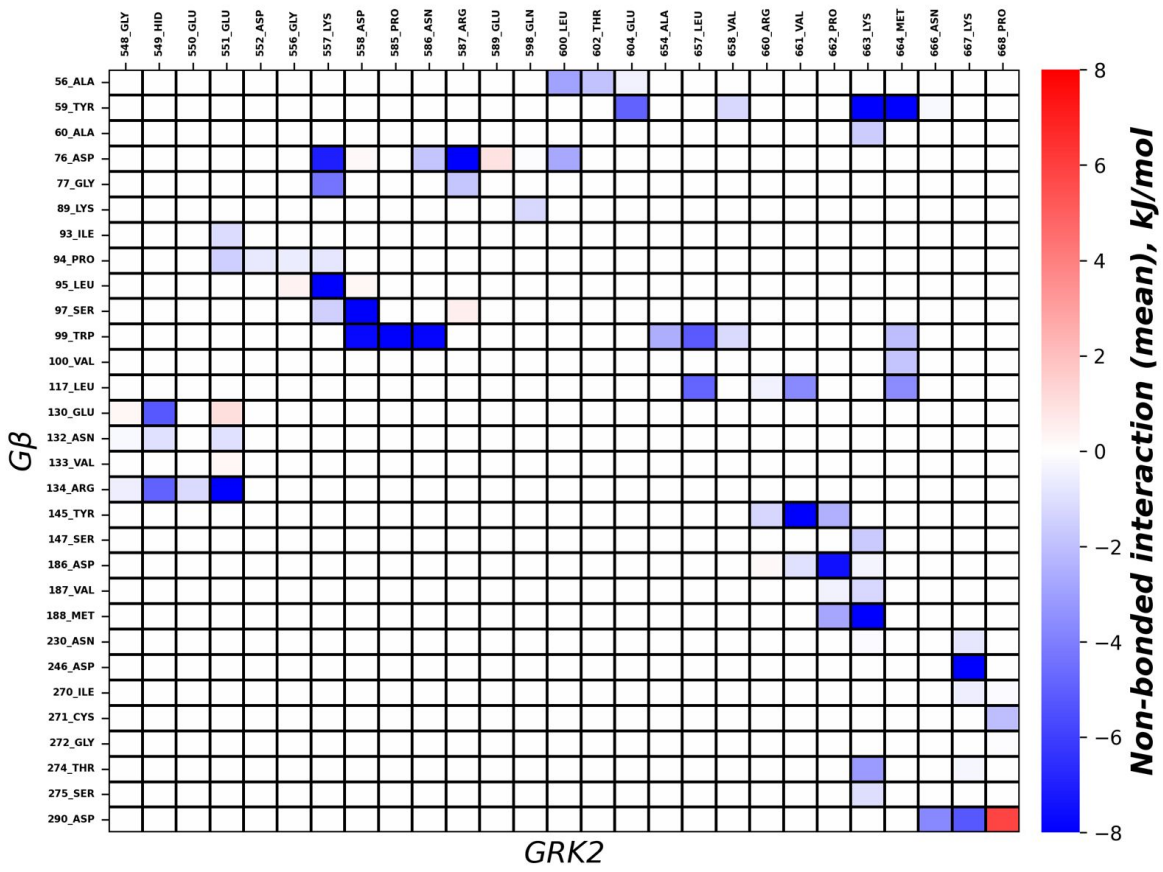

Figure 21: Mean non-bonded interactions between $G\beta_1$ and GRK2, computed over 10 ns MD simulation time. Blue: stabilising effect; red: destabilising effect.

5. Discussion

The aim of this thesis was to investigate whether the A92T mutation leads to alterations in the binding behaviour of $G\beta_1\gamma_2$ with $G\alpha_i$ as well as GRK2, since they convey important actions in G protein signalling such as downstream effector activation and signal termination, respectively. Elbashat (2025) already provided important data in his master's thesis, suggesting no significant effect of the A92T mutation on $G\beta_1\gamma_2$ dimer formation, thus laying the foundation for this and future work.

As shown in Table 2, the average ΔΔG for the $G\alpha_iG\beta_1\gamma_2$ complex was calculated to be 4.25 kJ/mol, which is only slightly above an unsigned error threshold of 4 kJ/mol inherent to pmx free energy calculations [28]. Nonetheless, this positive value indicates a minor destabilising effect of the mutation on the examined heterotrimer that could potentially lead to it being constitutively active as already implied by Lohmann et al. (2017). However, it is important to note that there are numerous variants of Gα subunits that may interact quite differently from the specific $G\alpha_i$ subunit investigated in the course of this thesis as well as $G\alpha_{olf}$ examined by Lohmann et al. (2017). Thus, it will be crucial in future studies to investigate all relevant Gα subunits.

The average ΔΔG of -0.59 kJ/mol obtained for the $G\beta_1\gamma_2$GRK2 complex (Table 3) indicates no significant effect of the A92T variant on the interaction between the $G\beta_1\gamma_2$ dimer and GRK2. This is also supported by Figure 21, where no non-bonded interactions between A92 and GRK2 were found. These findings suggest that GRK2-mediated receptor phosphorylation and therefore downstream desensitisation will remain intact in this mutant. Of note, this is not the case for all disease-linked $G\beta_1$ positions, which warrants in-depth future investigation including ΔΔG calculations, as performed in this thesis for $G\alpha_iG\beta_1\gamma_2$.

Figure 10 illustrates the results of all three ΔΔG calculations performed for the A92T mutation so far in a coherent way. The plotting of the average ΔΔG values and standard deviations clearly shows similar results for the $G\beta_1\gamma_2$ dimer and the $G\beta_1\gamma_2$GRK2 complex, suggesting that the mutation has no significant effect on the stability of either structures. However, for the $G\alpha_iG\beta_1\gamma_2$ complex a change in energy of the states during the transformation of $G\beta_1\gamma_2$ into $G\alpha_iG\beta_1\gamma_2$ (4.57 kJ/mol) and $G\beta_1\gamma_2$GRK2 into $G\alpha_iG\beta_1\gamma_2$ (4.84 kJ/mol) is observed, exceeding the average kinetic energy of the particles at a temperature of 310 K (3.9 kJ/mol). Such a change in energies between the states can serve as a factor in the destabilisation of the $G\alpha_iG\beta_1\gamma_2$ heterotrimer, consistent with the results published by Lohmann et al. (2017).

As depicted in Figure 11, RMSD values for the $G\alpha_i$ subunit in complex with the mutant are higher than wild-type values. This implies increased structural flexibility and reduced conformational stability of the observed chain compared to the wild type complex. These findings correlate with the results from the free energy calculations, and confirm the

destabilising effect the mutation has on the G protein. RMSD calculations for the $G\beta_1$ subunit (shown in Figure 12) revealed elevated structural flexibility for the mutant from 25 ns until approximately 140 ns of simulation time, even displaying deviations of almost 0.4 nm, while the wild type exhibits relative conformational stability over the whole simulation time of 250 ns.

The RMSF analysis illustrated in Figure 13 shows comparable fluctuation profiles between the $G\beta_1$ wild type and the A92T variant, indicating that the mutation does not induce significant structural alterations within the $G\beta_1$ chain. Small changes can be seen around residues 174-216, 232, 288-306, and 342-344.

Analysis of non-bonded interactions of $G\beta_1$ with water shows substantially different results for the mutant and wild type protein. Considering the change in amino acids from hydrophobic alanine to somewhat hydrophilic threonine, these findings are reasonable. Residue energy analysis conducted for $G\alpha_i$ revealed four residues in the α_i chain that interact with residue 92 in the β_1 chain, though no significant changes in interaction energies have been found between the wild type and mutant. Results for neighbouring residues in $G\beta_1$ on the other hand show in part considerable shifts. Most noteworthy are the changes in interaction energies for residues 131, 132, and 133, for which the wild type shows values of approximately -12 kJ/mol to -19 kJ/mol for non-bonded interactions, while the mutant exhibits almost none. Since Elbashat (2025) did not detect significant free energy changes when looking at the $G\beta_1\gamma_2$ dimer alone, these shifts are likely induced by interactions with the $G\alpha_i$ subunit.

In summary, the results of the simulations computed as part of this thesis highlight the changes in $G\alpha_iG\beta_1\gamma_2$ interactions caused by the A92T mutation. $\Delta\Delta G$ results are indicative of a loss in stability of this specific complex, confirmed by RMSD calculations. However, the calculated effects are rather mild, which might be due to the specific Gα subunit examined, and the relatively short simulated runs (10 ns). Overall, the results coincide with the experimental data obtained by Lohmann et al. (2017) for the $G\alpha_{olf}G\beta_1\gamma_7$ trimer.

Future research on the A92T mutation should focus on investigating different Gα subunits as well as other downstream effector molecules that might reveal greater structural disruption. Since in other *GNB1* variants epilepsy has been linked to disrupted interactions with GIRK channels [15], this might be a promising target to study as well. In general, the moderate effects on $G\alpha_i$ destabilisation cannot fully explain the broad phenotype of the patient, including dystonia and seizures. Manifestation of certain phenotypes such as dystonia is not yet clear and warrants further investigation both computationally and experimentally.

6. Conclusion

GNB1-E is a rare neurodevelopmental disorder, consequently little data is available on the pathophysiological impact of the disease-causing mutations. However, specific contributions such as the MD simulations carried out as part of this thesis can provide useful insights on structural and dynamic effects of certain mutations.

Knowledge on the pathology of *GNB1*-E is continuously growing, and this thesis contributes to a better understanding of the alterations that the A92T variant causes on a molecular level. Future research may explore the mutation's effects on other signalling pathways via effector proteins different from GRK2, or the consequences of a constitutively active Gα protein.

The more information that is gathered, the more precise treatment options can be developed. Currently, therapy is limited to symptom control, but recent advantages in CRISPR/Cas9 technology provide the theoretical possibility of single-nucleotide corrections, potentially enabling personalised gene therapies tailored to specific mutations. However, a crucial limitation of these technologies is the time factor: Since *GNB1*-E is a neurodevelopmental disease, treatment should start very early in order to obtain optimal therapy for affected patients. Thus, especially for older patients, drug repurposing or *de novo* drug development strategies might offer more promising treatment options.

7. Bibliography

[1] K. Lohmann, I. Masuho, D. N. Patil, H. Baumann, E. Hebert, S. Steinrücke, D. Trujillano, N. K. Skamangas, V. Dobricic, I. Hüning, G. Gillessen-Kaesbach, A. Westenberger, D. Savic-Pavicevic, A. Münchau, G. Oprea, C. Klein, A. Rolfs and K. A. Martemyanov, "Novel GNB1 mutations disrupt assembly and function of G protein heterotrimers and cause global developmental delay in humans," *Human Molecular Genetics,* vol. 26, no. 6, pp. 1078-1086, 15 March 2017.

[2] J. D. Da Silva, M. D. Costa, B. Almeida, F. Lopes, P. Maciel and A. Teixeira-Castro, "Case Report: A Novel GNB1 Mutation Causes Global Developmental Delay With Intellectual Disability and Behavioral Disorders," *Frontiers in Neurology,* no. 12, 27 September 2021.

[3] K. Szczałuba, A. Biernacka, K. Szymańska, P. Gasperowicz, J. Kosińska, M. Rydzanicz and R. Płoski, "Novel GNB1 de novo mutation in a patient with neurodevelopmental disorder and cutaneous mastocytosis: Clinical report and literature review," *European Journal of Medical Genetics,* vol. 61, no. 3, pp. 157-160, March 2018.

[4] "G-Proteins and Their Molecular Targets," in *Neuroscience*, 2nd ed., Sunderland, MA: Sinauer Associates, 2001.

[5] A. V. Smrcka, "G protein βγ subunits: Central mediators of G protein-coupled receptor signaling," *Cellular and Molecular Life Sciences,* vol. 65, pp. 2191-2214, 19 May 2008.

[6] S. M. Khan, R. Sleno, S. Gora, P. Zylbergold, J.-P. Laverdure, J.-C. Labbé, G. J. Miller and T. E. Hébert, "The Expanding Roles of Gβγ Subunits in G Protein–Coupled Receptor Signaling and Drug Action," *Pharmacological Reviews,* vol. 65, no. 2, pp. 545-577, April 2013.

[7] B. Rysiewicz, E. Błasiak, P. Mystek, M. Dziedzicka-Wasylewska and A. Polit, "Beyond the G protein α subunit: investigating the functional impact of other components of the Gαi3 heterotrimers," *Cell Communication and Signaling,* vol. 21, no. 1, 10 October 2023.

[8] D. J. Dupré, M. Robitaille, R. V. Rebois and T. E. Hébert, "The Role of Gβγ Subunits in the Organization, Assembly, and Function of GPCR Signaling Complexes," *Annual Review of Pharmacology and Toxicology,* vol. 49, pp. 31-56, February 2009.

[9] W. Müller-Esterl, Biochemie, 3 ed., Springer Spektrum, 2018.

[10] D. T. Lodowski, J. A. Pitcher, W. D. Capel, R. J. Lefkowitz and J. J. G. Tesmer, "Keeping G Proteins at Bay: A Complex Between G Protein-Coupled Receptor Kinase 2 and Gβγ," *Science,* vol. 300, no. 5623, pp. 1256-1262, 23 May 2003.

[11] C.-C. Han, Y. Ma, Y. Li, Y. Wang and W. Wei, "Regulatory effects of GRK2 on GPCRs and non-GPCRs and possible use as a drug target (Review)," *International Journal of Molecular Medicine,* vol. 38, no. 4, pp. 987-994, October 2016.

[12] M. Nasvytis, J. Čiauškaitė and G. Jurkevičienė, “GNB1 Encephalopathy: Clinical Case Report and Literature Review,” *Medicina,* vol. 60, no. 4, 1 April 2024.

[13] “What is GNB1 Syndrome?,” [Online]. Available: https://www.gnb1.org/diagnosis1. [Accessed 6 September 2025].

[14] P. Hemati, A. Revah-Politi, H. Bassan and et al., “Refining the phenotype associated with GNB1 mutations: Clinical data on 18 newly identified patients and review of the literature,” *American Journal of Medical Genetics,* vol. 176, no. 11, pp. 2259-2275, September 2019.

[15] H. P. Reddy, D. Yakubovich, T. Keren-Raifman, G. Tabak, V. A. Tsemakhovich, M. H. Pedersen, B. Shalomov, S. Colombo, D. B. Goldstein, J. A. Javitch, A. K. Bera and N. Dascal, “Encephalopathy-causing mutations in Gβ1 (GNB1) alter regulation of neuronal GIRK channels,” *iScience,* vol. 24, no. 9, 24 September 2021.

[16] W. Endo, S. Ikemoto, N. Togashi, T. Miyabayashi, E. Nakajima, S.-i. Hamano, M. Shibuya, R. Sato, Y. Takezawa, Y. Okubo, T. Inui, M. Kato, T. Sengoku, K. Ogata, K. Hamanaka, T. Mizuguchi, S. Miyatake, M. Nakashima, N. Matsumoto and K. Haginoya, “Phenotype–genotype correlations in patients with GNB1 gene variants, including the first three reported Japanese patients to exhibit spastic diplegia, dyskinetic quadriplegia, and infantile spasm,” *Brain & Development,* vol. 42, no. 2, pp. 199-204, 14 November 2019.

[17] L. Schultz-Rogers, I. Masuho, F. Pinto e Vairo, C. T. Schmitz, T. L. Schwab, K. J. Clark, L. Gunderson, P. N. Pichurin, K. Wierenga, K. A. Martemyanov and E. W. Klee, “Haploinsufficiency as a disease mechanism in GNB1-associated neurodevelopmental disorder,” *Molecular Genetics & Genomic Medicine,* vol. 8, no. 11, 12 September 2020.

[18] A. Revah-Politi, T. T. Sands, S. Colombo, D. B. Goldstein and K. Anyane-Yeboa, “GNB1 Encephalopathy,” Seattle, 2020.

[19] S. Petrovski, S. Küry, C. T. Myers and et al., “Germline De Novo Mutations in GNB1 Cause Severe Neurodevelopmental Disability, Hypotonia, and Seizures,” *The American Journal of Human Genetics,* vol. 98, no. 5, pp. 1001-1010, 5 May 2016.

[20] J. Peng, Y. Wang, F. He, C. Chen, L.-W. Wu, L.-F. Yang, Y.-P. Ma, W. Zhang, Z.-Q. Shi, C. Chen, K. Xia, H. Guo, F. Yin and N. Pang, “Novel West syndrome candidate genes in a Chinese cohort,” *CNS Neuroscience & Therapeutics,* vol. 24, no. 12, pp. 1196-1206, 18 November 2018.

[21] G. M. Conti, F. Cancellieri, M. Quinodoz, K. Kaminska, V. Vaclavik, C. Rivolta and H. V. Tran, “GNB1-Related Rod-Cone Dystrophy: A Case Report,” *Case Reports in Ophthalmology,* vol. 15, no. 1, p. 230–237, 18 March 2024.

[22] X.-R. Yang, F. Kassam and A. M. Innes, “Rod-cone dystrophy in an adult with GNB1-related disorder: An expansion of the phenotype and natural history,” *American Journal of Medical Genetics Part C: Seminars in Medical Genetics,* vol. 193, no. 2, pp. 183-187, 22 May 2023.

[23] A. Yoda, G. Adelmant, J. Tamburini and et al., “Mutations in G protein beta subunits promote transformation and kinase inhibitor resistance,” *Nature Medicine,* vol. 21, pp. 71-75, January 2015.

[24] M. Brett, A. H. M. Lai, T.-W. Ting, A.-M. Tan, R. Foo, S. Jamuar and E.-C. Tan, “Acute lymphoblastic leukemia in a child with a de novo germline gnb1 mutation,” *American Journal of Medical Genetics Part A,* vol. 173, no. 2, pp. 550-552, 19 January 2017.

[25] M. J. Betts and R. B. Russell, “Amino Acid Properties and Consequences of Substitutions,” in *Bioinformatics for Geneticists*, John Wiley & Sons, Ltd, 2003, pp. 289-316.

[26] J. J. Sajkowska, C. H. Tsang and P. Kozielewicz, “Application of FRET- and BRET-based live-cell biosensors in deorphanization and ligand discovery studies on orphan G protein-coupled receptors,” *SLAS Discovery,* vol. 29, no. 6, p. 100174, 29 July 2024.

[27] Y. Wu, N. Jensen, M. J. Rossner and M. C. Wehr, “Exploiting Cell-Based Assays to Accelerate Drug Development for G Protein-Coupled Receptors,” *International Journal of Molecular Science,* vol. 25, no. 10, p. 5474, 17 May 2024.

[28] M. Aldeghi, B. L. de Groot and V. Gapsys, “Accurate Calculation of Free Energy Changes upon Amino Acid Mutation,” in *Computational Methods in Protein Evolution. Methods in Molecular Biology*, vol. 1851, N. Y. N. Humana Press, Ed., 2019, pp. 19-47.

[29] D. Frenkel and B. Smit, Understanding Molecular Simulation: From Algorithms to Applications, 3. ed., C. Janco, Ed., Academic Press, Elsevier, 2023.

[30] E. Lindahl, “Molecular Dynamics Simulations,” in *Molecular Modeling of Proteins. Methods in Molecular Biology*, vol. 1215, N. Y. N. Humana Press, Ed., 2015, pp. 3-26.

[31] M. Elbashat, *Molecular Dynamic Simulation of A92T Mutation in Gβγ in case of GNB1 Encephalopathy,* Vienna, 2025.

[32] B. Shalomov, T. Friesacher, D. Yakubovich, J. C. Combista, H. P. Reddy, S. Dabbah, H. Bernsteiner, E.-M. Zangerl-Plessl, A. Stary-Weinzinger and N. Dascal, “Ethosuximide: Subunit- and Gβγ-dependent blocker and reporter of allosteric changes in GIRK channels,” *British Journal of Pharmacology,* vol. 182, no. 8, pp. 1704-1718, 12 March 2025.

[33] M. J. Abraham, T. Murtola, R. Schulz, S. Páll, J. C. Smith, B. Hess and E. Lindahl, “GROMACS: High performance molecular simulations through multi-level parallelism from laptops to supercomputers,” *SoftwareX,* Vols. 1-2, pp. 19-25, September 2015.

[34] “CHARMM-GUI,” Im Lab, Lehigh University, [Online]. Available: https://www.charmm-gui.org/. [Accessed January 2025].

[35] M. Whorton and R. MacKinnon, “PDB ID: 4KFM,” 2013. [Online]. Available: https://www.rcsb.org/structure/4KFM. [Accessed January 2025].

[36] M. Wall and S. Sprang, “PDB ID: 1GP2,” 1997. [Online]. Available: https://www.rcsb.org/structure/1GP2. [Accessed January 2025].

[37] D. Lodowski, J. Pitcher, W. Capel, R. Lefkowitz and J. Tesmer, “PDB ID: 1OMW,” 2003. [Online]. Available: https://www.rcsb.org/structure/1OMW. [Accessed January 2025].

[38] K. Lindorff-Larsen, S. Piana, K. Palmo, P. Maragakis, J. J. Klepeis, R. O. Dror and D. E. Shaw, “Improved side-chain torsion potentials for the Amber ff99SB protein force field,” *Proteins: Structure, Function, and Bioinformatics,* vol. 78, no. 8, pp. 1950 - 1958, 15 April 2010.

[39] “pmx protein web server,” 2022. [Online]. Available: http://pmx.mpibpc.mpg.de/webserver.html. [Accessed January 2025].

[40] G. E. Crooks, “Entropy production fluctuation theorem and the nonequilibrium work relation for free energy differences,” *Physical Review E,* vol. 60, no. 3, p. 2721, 1 September 1999.

[41] C. H. Bennett, “Efficient estimation of free energy differences from Monte Carlo data,” *Journal of Computational Physics,* vol. 22, no. 2, pp. 245-268, October 1976.

[42] “GitLab Anna Weinzinger's Lab,” [Online]. Available: https://gitlab.com/vihuhol188/g_beta_gamma_pmx. [Accessed 5 October 2025].